

## High-resolution imaging of bacterial spatial organization with vertical cell imaging by nanostructured immobilization (VerCINI)

Whitley, Kevin D.; Middlemiss, Stuart; Jukes, Calum; Dekker, Cees; Holden, Séamus

**DOI**

[10.1038/s41596-021-00668-1](https://doi.org/10.1038/s41596-021-00668-1)

**Publication date**

2022

**Document Version**

Accepted author manuscript

**Published in**

Nature Protocols

**Citation (APA)**

Whitley, K. D., Middlemiss, S., Jukes, C., Dekker, C., & Holden, S. (2022). High-resolution imaging of bacterial spatial organization with vertical cell imaging by nanostructured immobilization (VerCINI). *Nature Protocols*, 17(3), 847-869. <https://doi.org/10.1038/s41596-021-00668-1>

**Important note**

To cite this publication, please use the final published version (if applicable). Please check the document version above.

**Copyright**

Other than for strictly personal use, it is not permitted to download, forward or distribute the text or part of it, without the consent of the author(s) and/or copyright holder(s), unless the work is under an open content license such as Creative Commons.

**Takedown policy**

Please contact us and provide details if you believe this document breaches copyrights. We will remove access to the work immediately and investigate your claim.

1 **High-resolution imaging of bacterial spatial organisation with Vertical Cell Imaging by**  
2 **Nanostructured Immobilisation (VerCINI)**

3 Kevin D. Whitley<sup>1,2\*</sup>, Stuart Middlemiss<sup>1</sup>, Calum Jukes<sup>1</sup>, Cees Dekker<sup>2</sup>, Séamus Holden<sup>1\*</sup>

4 <sup>1</sup>Centre for Bacterial Cell Biology, Newcastle University, UK; <sup>2</sup>Department of Bionanoscience, Kavli  
5 Institute of Nanoscience Delft, Delft University of Technology, The Netherlands

6 \*Corresponding authors: [kevin.whitley@ncl.ac.uk](mailto:kevin.whitley@ncl.ac.uk), [seamus.holden@ncl.ac.uk](mailto:seamus.holden@ncl.ac.uk)

7

8 **ABSTRACT**

9 Light microscopy is indispensable for analysis of bacterial spatial organisation, yet the size and shapes  
10 of bacterial cells pose unique challenges to imaging. Bacterial cells are not much larger than the  
11 diffraction limit of visible light, and many species have cylindrical shapes and so lie flat on microscope  
12 coverslips, yielding low-resolution images when observing their short axes. In this protocol, we  
13 describe a pair of recently developed methods named VerCINI (Vertical Cell Imaging by Nanostructured  
14 Immobilisation) and  $\mu$ VerCINI (Microfluidic VerCINI) that greatly increase spatial resolution and image  
15 quality for microscopy of the short axes of bacteria. The concept behind both methods is that cells are  
16 imaged while confined vertically inside cell traps made from a nanofabricated mould. The mould is a  
17 patterned silicon wafer produced in a cleanroom facility using electron-beam lithography and deep  
18 reactive ion etching, which takes  $\sim 3$  hrs for fabrication and  $\sim 12$  hrs for surface passivation. After  
19 obtaining a mould, the entire process of making cell traps, imaging cells, and processing images can  
20 take  $\sim 2$ -12 hrs, depending on the experiment being done. VerCINI and  $\mu$ VerCINI are ideal for imaging  
21 anything along the short axes of bacterial cells, as they provide high-resolution images without any  
22 special requirements for fluorophores or imaging modalities, and can readily be combined with other  
23 imaging methods (e.g. STORM). VerCINI can easily be incorporated into existing projects by researchers  
24 with expertise in bacteriology and microscopy. Nanofabrication can be either done in-house, requiring  
25 specialist facilities, or outsourced based on this protocol.

26

27 **KEY REFERENCES USING THIS PROTOCOL**

28 Bisson-Filho, A. W. et al. *Science* **355**, 739-743 (2017): [10.1126/science.aak9973](https://doi.org/10.1126/science.aak9973)

29 Perez, A. J. et al. *Proc. Natl. Acad. Sci.* **116**, 3211-3220 (2019): [10.1073/pnas.1816018116](https://doi.org/10.1073/pnas.1816018116)

30 Whitley, K. D. et al. *Nat. Commun.* **12**, (2021): [10.1038/s41467-021-22526-0](https://doi.org/10.1038/s41467-021-22526-0)

31

32 **INTRODUCTION**

33 Although long underappreciated as amorphous sacks of enzymes, it is now clear that bacterial cells are  
34 highly spatially organized. How bacterial proteins dynamically organize and remodel large cellular  
35 structures such as the cell wall or the chromosome is a central question in bacteriology. However,  
36 imaging cellular spatial organisation and dynamics inside bacteria by light microscopy is challenging  
37 for several reasons. Firstly, bacteria are very small, with a typical diameter of  $1 \mu\text{m}$ , not much larger  
38 than the 250 nm diffraction limit of visible light. Secondly, most bacteria are not spherically symmetric,  
39 but exist in a wide range of shapes including rods and ovoids. During imaging, non-spherical bacteria

40 are usually immobilized flat on a microscope coverslip, with their long axes parallel to the imaging  
41 plane and their short axes orthogonal to the imaging plane (Figure 1a, top). Imaging structure and  
42 dynamics along the short axes is therefore difficult, both due to a significant amount of background  
43 signal from out-of-focus light and the fact that axial resolution is generally lower than lateral resolution  
44 (approximately 250 nm lateral vs 550 nm axial resolution<sup>1</sup>).

45 This is especially problematic when one considers that many bacterial processes occur, or are  
46 organized, along these shorter axes. For example, the peptidoglycan cell wall is primarily synthesized  
47 circumferentially around the cell during vegetative growth in many bacteria<sup>2-4</sup>. Similarly, when cells  
48 divide, their division machinery moves circumferentially around the cell septum to progressively  
49 synthesize the cell septum inwards<sup>5,6</sup>. When cells have divided, what was once the division plane  
50 becomes two daughter cell poles, which then also exist along the short axes of the cells. A large number  
51 of proteins localize specifically to the cell poles in rod-shaped bacteria that carry out a wide variety of  
52 functions, such as chemotaxis, motility, adhesion, virulence, chromosome organisation, cell-cycle  
53 regulation, and secretion<sup>7-11</sup>. A wealth of information on all these systems has been obtained from  
54 microscopy in recent years, but a major limitation remains that the horizontal orientation of cells is far  
55 from optimal for imaging these systems.

56 To address this problem we developed a method, termed Vertical Cell Imaging by Nanostructured  
57 Immobilisation (VerCINI), that enables high resolution light microscopy of any process organized along  
58 the short axes of bacterial cells by orienting cells vertically in nanofabricated cell traps<sup>5,12,13</sup>. We also  
59 developed a method for high-resolution imaging of the short axes of bacteria during fluid exchange  
60 termed Microfluidic VerCINI ( $\mu$ VerCINI)<sup>12</sup>. Here we provide a detailed practical guide to implementing  
61 both VerCINI and  $\mu$ VerCINI. We first give a general overview of the VerCINI method and its applications.  
62 We provide detailed workflows for all aspects of VerCINI and  $\mu$ VerCINI, from nanofabrication of  
63 micropillar arrays to acquisition and analysis of microscopy data. We provide rationales for the  
64 procedures described and include tips from our own experience in developing and using the methods  
65 to assist interested researchers. We also provide quantitative analysis of critical steps in the method  
66 to support troubleshooting and to enable future extensions and adaptations of the technique to new  
67 applications. By following the procedures described, this article should allow interested researchers to  
68 easily apply VerCINI to their own research.

## 69 **Development of the protocol**

70 We recently developed two methods that enable high resolution imaging of bacteria along their short  
71 axes by orienting them vertically in nanofabricated cell traps<sup>5,12,13</sup>. In the first method, VerCINI, cells  
72 are confined in nanofabricated 'microhole' arrays formed in an agarose pad such that the short axes  
73 of the cell are aligned to the microscope imaging plane, allowing much higher resolution images of the  
74 cell short axis than is possible with conventional immobilisation (Figures 1a and 2a, bottom). In the  
75 second method, termed Microfluidic VerCINI ( $\mu$ VerCINI), the microhole arrays are open-topped, and  
76 the vertically trapped cells are confined within a microfluidic chamber to enable rapid solution  
77 exchange and chemical perturbation (Figure 3a). Both methods were originally developed to trap rod-  
78 shaped bacterial cells, which include the majority of model systems (e.g. *Bacillus subtilis* and  
79 *Escherichia coli*) and many human pathogens (e.g. *Mycobacterium tuberculosis*). However, they are  
80 suitable for any cells with cylindrical symmetry, which also includes ovococcal species such as the  
81 human pathogen *Streptococcus pneumoniae*.

82 The key principle behind VerCINI is to rotate the short axes of bacteria into the microscope image plane  
83 by trapping cells in narrow microholes formed from either agarose or PDMS (Figures 1a, 2a, and 3a).  
84 In order to trap cells vertically, a silicon micropillar array serving as a negative master of the microholes

85 must be fabricated at sufficient resolution for precise and reproducible cell trapping. In standard  
86 VerCINI, this micropillar array is used as a mould to form a microhole array in agarose. Bacteria are  
87 then immobilized within the traps, imaged using a high-resolution inverted microscope, and data  
88 analysed using custom image processing software tailored to maximise SNR of VerCINI microscopy  
89 data.  $\mu$ VerCINI uses the same principle as standard VerCINI, but additionally enables rapid drug  
90 treatment of trapped cells by immobilizing bacteria in open-topped PDMS cell traps. VerCINI can also  
91 be easily combined with denoising, super-resolution microscopy, or single-particle tracking methods  
92 to further improve image quality or resolution.

### 93 **Advantages and limitations**

94 VerCINI and  $\mu$ VerCINI offer several benefits for imaging the short axes of cells compared to  
95 conventional imaging of horizontally oriented cells:

- 96 • *High resolution.* A slice across the plane with the short axes of the cell (e.g. the cell septum)  
97 can be viewed at high 250 nm resolution (Figure 1 bottom), rather than just a thin volume of  
98 the bottom of the cell (TIRF microscopy, Figure 1 top) or low 550 nm resolution imaging via  
99 3D fluorescence microscopy.
- 100 • *Simultaneous imaging of an entire slice of the cell short-axes plane.* An entire slice of the plane  
101 with the short axes of the cell can be imaged at once. Proteins that are primarily moving  
102 circumferentially, e.g. divisome or elongasome proteins, can then be tracked for extended  
103 periods<sup>12</sup>, unlike TIRF, which truncates protein trajectories due to its small illumination  
104 volume.
- 105 • *High signal-to-noise ratio (SNR) imaging of the cell poles.* By rotating cells vertically, the cell  
106 pole is placed in contact with/near to the microscope coverslip, and is also oriented to the  
107 microscope image plane. This allows high SNR imaging of the cell poles via TIRF illumination,  
108 while at the same time improving spatial resolution. Below, we demonstrate proof of concept  
109 application of VerCINI to imaging of cell pole protein dynamics (Figure 2).

110 Limitations to VerCINI and  $\mu$ VerCINI include the following:

- 111 • *Incompatible with long or chained cells.* Cells that are filamentous or form long unseparated  
112 chains are not likely to fit in the holes. In some cases these issues can be rectified with  
113 appropriate genetic modifications: for example, we have found that deleting the *hag* gene  
114 (encoding flagellin) or *slrR* gene (encoding a transcriptional regulator<sup>14</sup>) in the *B. subtilis* PY79  
115 background greatly reduces the presence of long unseparated chains of cells, enabling efficient  
116 loading into holes<sup>12</sup>.
- 117 • *Difficult to use with cells lacking cylindrical symmetry.* Although curved cells such as  
118 *Caulobacter crescentus* can be loaded into the microholes, data analysis for such cells can be  
119 complicated by the fact that the long (curved) axis of the cell is not parallel to the (straight)  
120 axis of the microscope, except at the cell mid-plane. One possibility to rectify this may be to  
121 first straighten such cells by deleting genes giving them curvature (e.g. *creS* in *C. crescentus*).
- 122 •  *$\mu$ VerCINI requires some non-standard microscope parts.* Due to the layer of PDMS between  
123 the microscope coverslip and vertically-trapped cells, imaging with this method currently  
124 requires a special objective lens and non-standard autofocus system. The specific reasons for  
125 this limitation and possible solutions are discussed in further detail in the Experimental Design  
126 section.

### 127 **Applications**

128 A key application for VerCINI is imaging the circumferential dynamics of cell division proteins. The  
129 septal peptidoglycan synthesis machinery moves circumferentially around the cell to build the cell wall,  
130 guided by the essential cytoskeletal protein FtsZ<sup>5,12</sup>. With conventional imaging, the division plane is  
131 orthogonal to the microscope imaging plane (Figure 1a, top), and hence the dynamics of division  
132 proteins are difficult to observe due to the background signal from out-of-focus light coming from the  
133 rest of the division ring. This background signal can be largely removed using total internal reflection  
134 fluorescence (TIRF) illumination, which produces an evanescent wave that excites only the bottom  
135 100-200 nm of the cell, but this limits imaging to only a small slice of the division septum (Figure 1b-c,  
136 top). In contrast, VerCINI allows simultaneous imaging of the entire septum, and strongly reduces  
137 background signal, because the septum no longer overlaps itself axially.

138 Using an early prototype of VerCINI, we observed the circumferential dynamics of FtsZ of the model  
139 rod-shaped *Bacillus subtilis* around the full division ring at high resolution and discovered that FtsZ  
140 filaments treadmill in the living cell (Figure 1b-c, bottom)<sup>5</sup>. VerCINI has since found a variety of  
141 applications in cell division microscopy. Using an optimized version of VerCINI with increased SNR, we  
142 were able to image FtsZ dynamics at near-single-filament resolution throughout the *B. subtilis* division  
143 cycle, demonstrating that FtsZ filament condensation into a dense Z-ring drives a transition in FtsZ  
144 dynamics from a mixed population of mobile and immobile filaments to stable treading during  
145 constriction initiation and active septum building. With  $\mu$ VerCINI we were also able to demonstrate  
146 that the FtsZ-targeting antibiotic PC190723 totally arrests FtsZ filament motion within seconds (Figure  
147 3b-c). Beyond this, VerCINI has been applied to image division in several different bacterial species  
148 using a variety of imaging methods: the dynamics of FtsZ treading in the ovoid bacterial  
149 pathogen *Streptococcus pneumoniae*<sup>13</sup>, the organisation of FtsZ and FtsN in *Escherichia coli* using STED  
150 super-resolution imaging<sup>15</sup>, the division-associated cell wall synthase FtsI in *E. coli* using single-particle  
151 tracking<sup>16</sup>, and peptidoglycan synthesis during division and elongation in *S. pneumoniae* using dSTORM  
152 with fluorescently-labelled 'clickable' D-amino acids<sup>17</sup>.

153 VerCINI also has multiple applications to cellular systems beyond cell division. Since the cell wall is  
154 synthesized circumferentially in many bacteria, nearly any protein involved in these processes is an  
155 ideal candidate for investigation with VerCINI. For example, we are currently using single-particle  
156 tracking to image the circumferential motion of the elongation-associated cytoskeletal protein MreB  
157 in *B. subtilis* (unpublished). Another possible application of VerCINI is the bacterial nucleoid and  
158 associated proteins, which may show significant radial organisation due to the combined effects of  
159 transcription and translation<sup>18</sup>. The general concept of using vertical cell immobilisation to improve  
160 imaging resolution has also been applied successfully to eukaryotic systems, although both the  
161 microfabrication and microscopy approaches required there differ substantially due to the much larger  
162 cell size<sup>19-21</sup>.

163 We believe that a major potential application of VerCINI is the imaging of cell poles. Vertical orientation  
164 increases the spatial resolution of cell pole organisation, and high signal-to-noise imaging with TIRF  
165 illumination becomes uniquely possible as the cell pole is placed in contact with the microscope  
166 coverslip. To illustrate this we provide brief proof-of-concept demonstration of VerCINI to cell pole  
167 imaging by investigating the dynamics of the *B. subtilis* chemoreceptor protein TlpA (Figure 2;  
168 Supplementary Methods). TlpA is a chemoreceptor protein in *B. subtilis* that forms large clusters  
169 localized to both the base of division septa and cell poles (Figure 2a-b), likely due to a binding  
170 preference for regions of high membrane curvature<sup>22</sup>. With conventional imaging, the distribution and  
171 dynamics of these clusters are obscured by the signal from overlapping clusters (Figure 2b, top). In  
172 contrast, orienting cells vertically with VerCINI and illuminating via TIRF allows for high resolution, high  
173 SNR imaging of these clusters at cell poles (Figure 2b-d). We observed that TlpA forms multiple large,

174 essentially immobile clusters (generalized diffusion coefficient  $\langle K_{\alpha} \rangle = 5 \cdot 10^{-7} \pm 6 \cdot 10^{-7} \mu\text{m}^2/\text{s}^{\alpha}$   
175 (mean  $\pm$  SD) for the data shown in Figure 2) of varying size, consistent with large chemoreceptor arrays  
176 observed in other organisms by cryo-electron tomography<sup>23</sup> (Figure 2b-d, bottom).

177 This protocol was optimised using *B. subtilis* strain PY79, although it is applicable to a wide range of  
178 bacterial cell types. We have used it to image *B. subtilis* 168, *S. pneumoniae* D39<sup>13</sup>, *Corynebacterium*  
179 *glutamicum* RES 167, and *E. coli* MG1655 while others have used it to image *S. pneumoniae* strain  
180 R800<sup>17</sup>. This protocol should be generally applicable to any bacterial cell type with cylindrical  
181 symmetry. Preliminary VerCINI measurements of the curved, non-cylindrical *Caulobacter crescentus*  
182 also gave successfully trapped cells, indicating that VerCINI may be also applicable to other curved rod-  
183 like cells.

184

## 185 **Experimental design**

### 186 **Nanofabrication of micropillars.**

187 We use e-beam lithography and deep reactive ion etching (DRIE) to create the micropillars on a silicon  
188 wafer using an approach similar to Deshpande & Dekker (2018)<sup>24</sup>.

189 We designed square microholes, as we hypothesized that a deformable material like agarose should  
190 trap cells more efficiently than circular ones due to a small number of cell-microhole contact points,  
191 leading to a larger fit tolerance. The following protocol is therefore for an array-of-squares pillar  
192 pattern (Figure 4c).

193 Since each silicon wafer can easily be split into four quarters, we recommend making four identical  
194 patterns—one in each quadrant (Figure 4c)—to maximise the utility of the wafer. Although space is  
195 available on the wafer to accommodate larger arrays, we use an overall pattern size of  $\sim 1 \times 0.5 \text{ cm}^2$   
196 because the agarose pad that will eventually contain this pattern will need to be cut down prior to  
197 imaging to ensure sufficient oxygen delivery to trapped cells (see Figure 6avi).

198 When using VerCINI for the first time, we recommend making several columns of differently-sized  
199 pillars (Figure 4c) to later find the optimal size for your particular bacteria and growth conditions (for  
200 *B. subtilis* we have found that pillars of width 1.0-1.3  $\mu\text{m}$  work best). Importantly, we have found that  
201 the Bosch etching process shrinks the squares substantially (Figure 5a-b) from the designed widths due  
202 to some degree of ‘isotropic etching’ (i.e. undercutting the resist), and so the designed widths must be  
203 larger to compensate. The amount that pillars shrink during the Bosch etch depends on both the sizes  
204 of gaps between pillars (Figure 5c) and the duration of the Bosch etch. For gaps of 3.0-3.5  $\mu\text{m}$ , we have  
205 measured a decrease in widths of  $560 \pm 110 \mu\text{m}$  (mean  $\pm$  SD) for a 100 s Bosch etch (N=4 wafers) and  
206  $680 \pm 40 \mu\text{m}$  (mean  $\pm$  SD) for a 140 s Bosch etch (N=2 wafers). However, for a given gap size and Bosch  
207 etch time, we have found that the decrease in pillar widths is reproducible.

208 One other critical factor when designing the array-of-squares pattern is e-beam write time. Since it  
209 takes significantly more time for the e-beam system to move the sample stage than to deflect the  
210 beam, moving the stage to write each individual square shape will require a prohibitively long amount  
211 of time. However, the area over which the e-beam can write at a single stage position (the main field;  
212  $\sim 1 \times 10^6 \mu\text{m}^2$  for our Raith EBPG-5000+) is much larger than each individual square that will be written  
213 ( $\sim 1 \mu\text{m}^2$ ). So, the protocol below describes how to produce an array of squares that is roughly the same  
214 size as the e-beam’s main field, and then later replicate this array to obtain a larger array pattern. This  
215 way, thousands of squares are written at each stage position, dramatically reducing the e-beam write  
216 time.

217 One further consideration is the heights of pillars that will be needed. The optimal heights are mainly  
218 determined by the average length of cells that users want to eventually image in microholes (for *B.*  
219 *subtilis* we typically use pillars of height 4-7  $\mu\text{m}$ ). Pillars can also be made taller to accommodate longer  
220 cells or multiple short cells as a column, but taller (i.e. higher aspect ratio) pillars are more fragile and  
221 susceptible to breaking when agarose or polydimethylsiloxane (PDMS) are peeled off of them. We have  
222 successfully used pillars with aspect ratio up to  $\sim 10$  (1  $\mu\text{m}$  square pillars 10  $\mu\text{m}$  tall), but it is likely that  
223 pillars with much higher aspect ratios will not be feasible. To further prevent pillars breaking when  
224 PDMS is peeled off, we coat the wafers with a silane compound (tridecafluoro-1,1,2,2-tetrahydrooctyl  
225 trichlorosilane) by vapour deposition to prevent strong adhesion. Although designed to enable  
226 solidified PDMS to be removed, we also found that this silane coat makes solidified agarose peel off  
227 more easily as well.

228 For researchers that do not have access to a nanofabrication facility, silicon wafers for VerCINI can be  
229 fabricated commercially based on this protocol. We are currently performing prototyping and testing  
230 with ConScience AB, Sweden, to make VerCINI chips available to other researchers, without financial  
231 benefit to ourselves. ConScience have estimated production cost at \$2900 per wafer (\$700 per VerCINI  
232 chip). The authors or the company may be contacted for updates. Other companies should also be able  
233 to fabricate these devices.

#### 234 **Sample preparation and imaging**

235 To image cells during vegetative growth, VerCINI pads are made using agarose dissolved in growth  
236 media using an approach adapted from de Jong et al. (2011)<sup>25</sup>. The porous nature of the agarose gel  
237 allows nutrients to diffuse through to cells allowing continued growth during the imaging process,  
238 while a high agarose concentration makes the gel stiff, providing structural stability to the microholes.

239 One critical factor for VerCINI is the efficiency with which cells are loaded into holes. A higher loading  
240 efficiency corresponds to more trapped cells in a single FoV, and therefore greater data acquisition.  
241 We have found that centrifuging concentrated cell culture into the holes using a flat bottomed  
242 centrifuge rotor gives high loading efficiency (Figure 6c-d).

243 Another important consideration is that cells are sometimes poorly trapped in the holes, causing them  
244 to wobble (Supplementary Video 1). Although these are relatively rare for correctly sized micropillars,  
245 imperfectly-trapped cells can be identified and removed from further analysis by recording a short ( $\sim 1$   
246 s) bright-field video after fluorescence acquisition. We initially hypothesized that flagellar motility  
247 might cause this poor trapping. However, at least in *B. subtilis* this does not appear to be the case, as  
248 deleting the *hag* gene made little difference to the amount of poorly trapped cells. In the less chain-  
249 forming *B. subtilis* strain BS168 we frequently perform experiments in motility-proficient cells without  
250 issue.

251 After loading, cells can be imaged using any microscope technique suitable for studying bacterial  
252 spatial organisation. Importantly, microholes are imprinted on the top of the agarose pad, so the cells  
253 are adjacent to the coverslip surface (Figures 1b and 2b). This means that illumination techniques such  
254 as HILO (for cell sidewall; e.g. Figure 1b) and TIRF (for cell poles; e.g. Figure 2b) are preferable to  
255 maximize image signal to noise ratio (SNR). We employ a ring-TIRF or ring-HILO system, where  
256 galvanometer-driven mirrors rotate the illumination beam at high speed (200 Hz) to produce uniform  
257 illumination across the sample<sup>26</sup>, however single angle TIRF or HILO are also sufficient.

#### 258 **$\mu$ VerCINI**

259 In many experiments, researchers want to perform rapid solution exchange during imaging, either to  
260 change from one medium to another, to add perturbatives such as antibiotics, to fix cells, or to label  
261 cells with exogenous dyes. However, with the original VerCINI method this is not possible since the  
262 slide is closed and the cells are underneath a dense pad of agarose. We have therefore designed an  
263 adapted version of the method to be compatible with solution exchange, called microfluidic VerCINI  
264 ( $\mu$ VerCINI). In this method, the microholes are open-topped (Figure 3a), and the cells are exposed to a  
265 fluid environment that is controlled by users through a microfluidic system.

266 One critical difference with this open-topped orientation is that there is a layer of material between  
267 the coverslip surface and the cells through which imaging will be done. Making a thin layer with  
268 agarose is challenging, and imaging through a thick layer of agarose would lead to substantial loss in  
269 image quality due to scattering. We instead use PDMS, which forms a relatively thin ( $\sim 50 \mu\text{m}$ )  
270 transparent layer (Figure 7a).

271 Because the holes are formed of PDMS rather than agarose, loading cells into the holes of a  $\mu$ VerCINI  
272 coverslip differs somewhat from VerCINI. PDMS is normally quite hydrophobic, and the surface tension  
273 of an aqueous cell culture is high enough that the microholes will end up filled with air bubbles rather  
274 than liquid or cells. PDMS is therefore first rendered hydrophilic by treatment with oxygen or air  
275 plasma (Figure 7ci).

276 After cells are loaded, the  $\mu$ VerCINI coverslip is adhered to a pre-fabricated device (Figure 7b) to form  
277 a closed microfluidic chamber (Figure 7d). This device consists of a microscope slide with drilled holes  
278 to allow for inlet and outlet tubing, along with a piece of double-sided tape that has been cut to form  
279 a flow channel. The double-sided tape serves two functions: it forms a thin ( $\sim 100 \mu\text{m}$ ) flow channel  
280 between the microscope slide and the tops of the microholes, and it seals the whole system together.  
281 It is important to identify a suitable double-sided tape as not all brands of double-sided tape adhere  
282 well to PDMS, which can produce leaks. We have found that Duck and Club brand double-sided tapes  
283 work well, while Scotch, Sellotape, and WHSmith double-sided tapes do not.

284 There are two key points to consider when imaging with  $\mu$ VerCINI. Firstly, even with a relatively thin  
285  $50 \mu\text{m}$  PDMS layer on top of a #1.5 microscope coverslip we found that we cannot successfully acquire  
286 images using a high N.A. oil immersion 100x TIRF objective. This is likely due to spherical aberration  
287 resulting from refractive index mismatch between PDMS ( $n=1.43$ ) and glass ( $n=1.52$ ). We instead use  
288 a silicone immersion oil objective since the silicone oil refractive index ( $n=1.41$ ) is similar to PDMS. This  
289 objective also has a large working distance (0.3 mm) which is useful for imaging through the PDMS  
290 layer.

291 Secondly,  $\mu$ VerCINI is not compatible with reflection-based autofocus systems. This is because very  
292 little reflection occurs off the PDMS/liquid interface, as the indices of refraction are too similar ( $\sim 1.43$   
293 and  $\sim 1.33$ , respectively). One possible solution is to use image-based autofocus methods (e.g. Micro-  
294 Manager's OughtaFocus), however these are not suitable for correcting drift during high-speed  
295 imaging of protein dynamics. A solution that we favour is to use an image-based autofocus system that  
296 measures drift using the cross-correlation between images and a reference stack in a separate infrared  
297 bright-field illumination and imaging pathway<sup>27</sup>. We developed a custom plugin for Micro-Manager to  
298 set the reference stack, calculate the cross-correlation maps, and maintain sample focus by closed-  
299 loop positioning of the microscope stage<sup>12</sup>. We perform the IR drift correction method on a custom  
300 built high resolution microscope, but the apparatus for this method can also be retrofitted onto  
301 commercial microscopes<sup>27</sup>. If automated drift correction methods are not available, with practise it is  
302 possible for a skilled operator to continuously manually correct for drift during image acquisition.



303 However, this will usually lead to reduced image quality due to increased periods of defocus during  
304 data acquisition.

305 It is also important to note that—unlike VerCINI— $\mu$ VerCINI is often used for ‘single-shot’ experiments,  
306 which limits users to recording a single field of view. For example, if a researcher wants to image the  
307 effect of an antibiotic perturbation on protein dynamics inside cells (e.g. Figure 3c), then the  
308 experiment can’t be repeated on a different field of view with the same slide, as all cells on the slide  
309 have already been perturbed. Because of this it is imperative not only to have high loading efficiency,  
310 but also to take some time to scan across the slide and find the best possible field of view before  
311 beginning.

## 312 **Image processing and analysis**

313 We focus here on our most common VerCINI image analysis use case: analysis of protein motion  
314 around the cell circumference or cell septum via kymograph analysis. This analysis method is  
315 appropriate when protein motion is mostly restricted to the leading edge of the cell septum (e.g. FtsZ)  
316 or the cell sidewall (e.g. MreB or other elongasome proteins). For other datasets, such as TIRF imaging  
317 of cell pole-localized proteins, other analysis methods such as single molecule tracking may be more  
318 appropriate. The overall workflow for image processing and analysis is shown in Figure 8a.

319 The first steps of image processing are done in Fiji/ImageJ<sup>28</sup>. We have developed a plugin called  
320 VerciniAnalysisJ specifically for processing VerCINI videos, which can be installed from the  
321 VerciniAnalysisJ update site with all its dependencies. Later image processing steps such as subtracting  
322 the cytoplasmic background signal and producing kymographs are done in MATLAB. We have  
323 developed software for these steps in a package called ring-fitting2 that is publicly available on  
324 GitHub<sup>29</sup>.

325 Two key processing steps are image denoising and registration. We found that image denoising allows  
326 us to substantially reduce illumination intensity while still maintaining high signal to noise ratio,  
327 thereby minimizing photobleaching and phototoxicity. We strongly recommend denoising VerCINI  
328 data prior to subsequent analysis. While a number of denoising algorithms have been developed, we  
329 use the ImageJ plugin PureDenoise, which is based on wavelet decomposition<sup>30</sup>. One advantage to  
330 using this algorithm is that it does not make any assumptions about the underlying biological structure.  
331 After denoising, any global image drift—for example due to agarose contraction—is corrected via  
332 image registration using the ImageJ plugin StackReg<sup>31</sup>.

333 Our *ring-fitting2* software automatically extracts kymographs of circumferentially localised protein  
334 dynamics<sup>12</sup> (Figure 8d-e). This software also subtracts the diffuse out-of-focus cytoplasmic background  
335 (Figure 8d), which can otherwise obscure protein dynamics. The background signal is subtracted from  
336 the image stack for each frame, and then the intensity around the fitted circle is calculated to sub-pixel  
337 precision via interpolation. We found that sub-pixel fitting of the cell centre and septum/  
338 circumference and robust background subtraction were crucial to obtaining accurate intensity  
339 measurements. During software development, we observed that small inaccuracies in cell centre  
340 localisation, caused for example by fitting an annulus with uniform instead of sectorised amplitude  
341 would cause large errors in apparent septal intensity as the small size of the cell, together with the  
342 complex background meant that different amounts of background signal would be integrated on either  
343 side of the cell. In order to confirm that the microscope system and image processing pipeline are  
344 together giving even circular symmetric intensity measurements around the centre of the cell, a cell  
345 expressing cytoplasmic GFP can be imaged and analysed. An example script for this purpose is supplied  
346 in the VerCINI analysis software.

347 Processive protein motion is visible on kymographs as a diagonal line, with line angle indicating protein  
348 speed. For dense protein filaments such as FtsZ, we currently quantify protein speed, bound lifetime,  
349 and other parameters such as directional switching and pausing by manual kymograph annotation  
350 (Figure 8g-h), as we found that most automated kymograph annotation methods do not perform well  
351 at high density. An ImageJ macro is provided for quantification of filament dynamics via manual ImageJ  
352 regions of interest (ROIs) annotation. During kymograph analysis, it can be difficult to identify  
353 trajectories of dim filaments due to the large intensity range within kymographs. This issue is  
354 frequently encountered for analysis of FtsZ dynamics in dense Z-rings. To address this issue, we  
355 recommend applying a ridge detection filter to the kymograph, which detects peaks within an image  
356 irrespective of intensity based on the image second derivative. A script '*Ridge\_Filter.ijm*' is provided  
357 for this purpose. We note that a recent deep learning based kymograph annotation tool could enable  
358 automated processing of VerCINI kymographs in the future<sup>32</sup>.

### 359 **Level of expertise needed to implement the protocol**

360 The nanofabrication protocol we describe to obtain a micropillar silicon wafer requires a cleanroom  
361 facility with appropriate training. This requirement can be avoided by ordering commercially fabricated  
362 wafers. Once a micropillar wafer is available, the rest of the VerCINI/ $\mu$ VerCINI protocol can be  
363 performed in any bacteriology lab with expertise in live single cell resolution fluorescence microscopy.  
364 Although  $\mu$ VerCINI does not require prior expertise in soft lithography or microfluidics, it is more  
365 difficult than VerCINI due to some specialized hardware and more complicated assembly. We therefore  
366 recommend users to become experienced at using VerCINI prior to trying  $\mu$ VerCINI.

367

## 368 **MATERIALS**

### 369 **REAGENTS**

- 370 • Silicon wafer (4-inch diameter, 500  $\mu$ m thickness, one side polished, type/orientation  
371 NP<100>, PB<100>, resistivity 1-10  $\Omega$ -cm; International Wafer Service)
- 372 • 1,1,1,3,3,3-hexamethyldisilazane (HMDS; VWR, cat. no. 51152885). CAUTION: This  
373 compound is highly flammable and is toxic on contact with skin or if inhaled. Wear protective  
374 gloves, protective clothing, eye protection, and face protection.
- 375 • Negative e-beam resist (e.g. AR-N-7700.18; Allresist)
- 376 • Developer (e.g. Microposit MF-321; micro resist technology)
- 377 • (Tridecafluoro-1,1,2,2-tetrahydrooctyl)trichlorosilane (abcr, cat. no. AB111444). CAUTION:  
378 This compound is flammable, and causes severe skin burns and eye damage. It reacts with  
379 water to produce hydrogen chloride. Wear protective gloves, protective clothing, eye  
380 protection, and face protection. Work in a dry, inert gas atmosphere while handling. Once  
381 aliquoted, flush the stock bottle with argon and seal the lid with parafilm.
- 382 • Ultrapure agarose (Invitrogen, cat. no. 16500-100)
- 383 • Polydimethylsiloxane (PDMS) elastomer base (Dow Corning, Sylgard 184 elastomer base)
- 384 • PDMS curing agent (Dow Corning, Sylgard 184 elastomer curing agent)
- 385 • Cell growth media (experiment-specific, but ideally should have low autofluorescence)

### 386 **BIOLOGICAL MATERIALS**

- 387 • *B. subtilis* SH130 (PY79  $\Delta$ hag ftsZ::*ftsZ-gfp-cam*)<sup>12</sup>.
- 388 • *B. subtilis* HS48 (168 *amyE::spc P<sub>xyI</sub>-tlpA-mgfp*)<sup>22</sup>.

## 389 EQUIPMENT

### 390 Cleanroom equipment

- 391 • Spin-coating system (SUSS MicroTec)
- 392 • Hot plates (Harry Gestigkeit, cat. no. 2860EB)
- 393 • Syringe (5 mL; e.g. BD Plastipak)
- 394 • Syringe filter (0.22 µm; e.g. Starlab)
- 395 • Electron-beam lithography system (Raith, model no. EBP5000+)
- 396 • Upright microscope (Olympus, model no. BX51M)
- 397 • Deep reactive ion etching system (Adixen; AMS, model no. 100 I-speeder)
- 398 • Stylus profilometer (Bruker, model DektakXT)
- 399 • Scanning electron microscope (e.g. FEI, NovaNano SEM)

### 400 Wet lab equipment

- 401 • Inert gas (e.g. argon) supply
- 402 • Vacuum desiccator (Kartell)
- 403 • Vacuum pump (Leybold Trivac, model no. D8B)
- 404 • Diamond scribe (e.g. RS Pro, Stock No. 394-217)
- 405 • Gene Frames (65 µL, 1.5 × 1.6 cm<sup>2</sup>; Thermo Scientific)
- 406 • Microwave
- 407 • Water bath with heater (e.g. Grant, model JB Nova)
- 408 • Mini-centrifuge (Eppendorf, model 5424)
- 409 • Silicone gaskets (Sigma-Aldrich, cat no. GBL103240), cut into individual 9 mm gaskets
- 410 • Centrifuge (VWR, model 5810, cat. no. EPPE5810000.060)
- 411 • Rotor with flat-bottomed buckets (VWR, A-4-81 Swing-out Rotor with 4 x MTP/Flex Buckets,
- 412 cat. no. 521-0145)
- 413 • Oven (e.g. Falc Instruments, Mini Oven STZ 5.4)
- 414 • Flat blade (e.g. Stanley 18 mm snap off blades, cat. no. 0-11-301)
- 415 • Power drill (e.g. Dremel, Dremel 4000)
- 416 • Multi-chuck for power drill (e.g. Dremel, 0.8-3.2 mm keyless chuck)
- 417 • Diamond-tipped drill bits (0.75 mm; Kingsley North, cat. no. 1-0500-100)
- 418 • Double-sided tape (e.g. Duck, 38 mm × 5 m)
- 419 • Pipette tips (e.g. Starlab, 10 µL)
- 420 • Polyethylene tubing (ID 0.38 mm, OD 1.09 mm; Smiths Medical, cat. no. 800/100/120)
- 421 • Rapid-drying epoxy (Araldite)
- 422 • Needles (0.45 mm × 10 mm (26g x 3/8"); BD Microlance)
- 423 • Plasma cleaner (Harrick Plasma, cat. no. PDC-002-CE)
- 424 • Syringe (20 mL; BD Plastipak)
- 425 • Syringe pump (Aladdin-220; World Precision Instruments)

### 426 Microscopy equipment

- 427 • Microscope slides (e.g. VWR Super Premium)
- 428 • Microscope coverslips (22 × 22 mm<sup>2</sup>, thickness no. 1.5; VWR)
- 429 • Inverted fluorescence microscope, preferably with laser-based total internal reflection
- 430 fluorescence (TIRF)/ highly inclined and laminated optical sheet (HILO) illumination (e.g.
- 431 Nikon N-STORM).

- 432 • 100× oil immersion objective (e.g. Nikon, CFI Apochromat TIRF 100XC Oil)
- 433 • 100× silicone oil immersion objective (Nikon, CFI SR HP Plan Apo Lambda S 100XC Sil, for
- 434  $\mu$ VerCINI only)
- 435 • Microscope incubation or stage heating device (for live cell microscopy)

## 436 SOFTWARE

- 437 • Computer-aided design (CAD) software (e.g. AutoCAD (Autodesk),
- 438 <https://www.autodesk.eu/products/autocad/overview>)
- 439 • BEAMER (GenISys, <https://www.genisys-gmbh.com/beamer.html>)
- 440 • Cjob (Vistec Lithography)
- 441 • Image acquisition software (e.g. Micro-Manager v2.0gamma, <https://micro-manager.org/>)
- 442 • Fiji v1.53 (<https://fiji.sc>)
- 443 • VerciniAnalysis ImageJ plugin (<https://github.com/HoldenLab/VerciniAnalysisJ>)
- 444 • MATLAB (Mathworks)
- 445 • ring-fitting2 MATLAB package (<https://github.com/HoldenLab/ring-fitting2>)

446

## 447 PROCEDURE

### 448 Design of an array-of-squares pattern. TIMING ~30 min – 2 hr

- 449 1. Make a  $1 \times 1 \mu\text{m}^2$  square in AutoCAD. Save it as a dxf file.
- 450 2. In BEAMER, make an array of squares the size of the e-beam main field. One possible algorithm to
- 451 achieve this is shown in Figure 4a.
  - 452 a. Input the dxf file containing the square.
  - 453 b. Use one loop to scale the square to a range of different sizes, as desired (e.g. 1.4-2.0  $\mu\text{m}$  edge
  - 454 lengths).
  - 455 c. Within this loop, use two more loops in series to make an array of squares in X and Y, selecting
  - 456 the option to merge the results of all loops rather than to only keep the final loop iteration.
  - 457 Arrays of each desired square size will be output as a separate gpf file. **?TROUBLESHOOTING.**
- 458 3. In Cjob, load the gpf files from BEAMER and replicate them several times to make four full arrays,
- 459 one in each quadrant of the wafer. Also add in identifiers and a solid rectangle to measure heights.
- 460 A code structure to achieve this is shown in Figure 4b.
  - 461 a. For Substrate, choose a 100 mm diameter silicon wafer and 100 kV exposure.
  - 462 b. Using Layout, replicate all patterns in each quadrant of the wafer to maximize its use (2x2).
  - 463 c. Again using Layout, replicate the gpf files from BEAMER to make a large array pattern in each
  - 464 wafer quadrant. We repeat the pattern 2x in the X direction and 5x in the Y direction. Select
  - 465 the following parameters for writing: dose =  $117 \mu\text{C}/\text{cm}^2$  (for AR-N-7700 resist), beam step
  - 466 size = 25 nm, beam size = 56 nm.
  - 467 d. Add identifiers around the entire array so that the sizes can be identified later under a
  - 468 microscope. Select the following parameters for writing: dose =  $117 \mu\text{C}/\text{cm}^2$ , beam step size
  - 469 = 50 nm, beam size = 95 nm.
  - 470 e. Add a solid  $1000 \times 500 \mu\text{m}^2$  rectangle above each array so that the heights can be measured
  - 471 with a profilometer after etching. Write the rectangle with the parameters: dose =  $117$
  - 472  $\mu\text{C}/\text{cm}^2$ , beam step size = 50 nm, beam size = 95 nm.
  - 473 f. Export the file as a job to the e-beam system.

### 474 Fabrication of a silicon micropillar wafer. TIMING ~3 hr

475 **CRITICAL:** Steps 4-10 should be performed in a cleanroom facility (for this work, a class 10,000  
476 (International Organization for Standardization (ISO) 7) facility with a class 100 (ISO 5) work area was  
477 used). These steps are adapted from Deshpande & Dekker (2018)<sup>24</sup>.

- 478 4. Spin-coat the wafer with negative e-beam resist.
- 479 a. Prime a 4-inch diameter silicon wafer by spreading ~5 mL HMDS on the polished side, and  
480 spin-coating it at 1000 rpm for 1 min. Immediately bake the wafer at 200°C for 2 min. HMDS  
481 will increase adhesion of the resist. (Prior to spin-coating, the wafer can optionally be cleaned  
482 with fuming nitric acid to remove dust and impurities. This is recommended to prevent non-  
483 uniform deposition of resist on the wafer during spin-coating and hence ensure that the  
484 patterns avoid defects arising from this. However, we have found that this step is typically  
485 unnecessary if fresh silicon wafers are used straight from packaging.)
- 486 b. Using a 0.22 µm filter, carefully spread ~5 mL of AR-N-7700.18 resist on the wafer. If bubbles  
487 appear, gently move them away from regions where patterns will be written using either the  
488 tip of the syringe filter or a cleanroom wipe. Spin-coat the wafer at 500 rpm for 1 min, then  
489 immediately bake at 85°C for 2 min. **?TROUBLESHOOTING.**
- 490 5. Write the array-of-squares micropillar pattern on the coated wafer using an electron-beam  
491 lithography system following the manufacturer's instructions.
- 492 6. Bake the wafer immediately after writing at 105°C for 2 min. **CRITICAL STEP:** Failure to bake the  
493 wafer will result in patterned region dissolving during development. **PAUSE POINT:** The baked  
494 wafer can be kept at room temperature (~22°C) in a dust-free environment indefinitely.
- 495 7. Develop the wafer to remove the resist that was not exposed to the e-beam.
- 496 a. Soak the wafer in MF-321 for 90 s and swirl gently.
- 497 b. Immediately, soak the wafer in diluted MF-321 solution (10% v/v MF-321 in water) for 30 s  
498 and swirl gently.
- 499 c. Immediately, soak the wafer in water for at least 30 s, swirling gently.
- 500 d. Dry the wafer.
- 501 e. Inspect the wafer under an upright light microscope at 60-100× magnification to ensure  
502 patterns have developed properly. **PAUSE POINT:** The developed wafer can be kept at room  
503 temperature in a dust-free environment indefinitely. **?TROUBLESHOOTING.**
- 504 8. Etch the wafer using a Bosch process in an AMS 100 I-Speeder to produce vertical pillars, then  
505 remove the remaining resist with O<sub>2</sub> plasma.
- 506 a. Clean the chamber of the inductively coupled plasma (ICP) reactive ion etcher for 20 min prior  
507 to beginning. Using O<sub>2</sub> gas set to 200 standard cubic centimeters per min (SCCM) with ICP  
508 power set to 1800 W and biased power set to 60 W.
- 509 b. Place the wafer in the etcher and set the following parameters: wafer temperature = 10°C,  
510 chamber pressure = 0.04 mbar, source-target distance = 200 mm.
- 511 c. Etch the wafer using a Bosch process. The etching step is 200 SCCM SF<sub>6</sub> for 7 s with ICP power  
512 set to 2000 W and capacitive coupled plasma (CCP) power at 0 W. The passivation step is 80  
513 SCCM C<sub>4</sub>F<sub>8</sub> for 3 s with ICP power set to 2000 W and CCP power in chopped low-frequency  
514 bias mode: 80 W for 10 ms and 0 W for 90 ms. The etching time depends on the desired  
515 structure height (see Figure 5d for guide).
- 516 d. Remove the resist with the AMS 100 I-speeder using O<sub>2</sub> gas at 200 SCCM for 10 min with the  
517 following parameters: wafer temperature = 10°C, chamber pressure = 0.04 mbar, source-  
518 target distance = 200 mm, ICP power = 2500 W with biased power = 50 W.
- 519 9. Measure the height of the etched structures by moving the stylus of a DektakXT profilometer over  
520 the 1000 × 500 µm<sup>2</sup> rectangle in the pattern.

521 10. Inspect the true widths of the pillars with a scanning electron microscope. **PAUSE POINT:** The  
522 silicon wafer can be kept at room temperature indefinitely.

523 **Passivation and dicing of the silicon micropillar wafer. TIMING ~12 hr**

- 524 11. Passivate the silicon micropillar wafer with a silane compound using vapour deposition.  
525 a. Evacuate air in a glass desiccator with argon to remove moisture.  
526 b. Pipette 10  $\mu\text{L}$  of (tridecafluoro-1,1,2,2-tetrahydrooctyl)trichlorosilane into a tube in the  
527 desiccator. Leave the tube open.  
528 c. Place the wafer in the desiccator. Pull vacuum in desiccator down to  $\sim 10$  mbar.  
529 d. Close the desiccator valve and turn off the vacuum.  
530 e. Remove wafer after  $\sim 12$  hr. **PAUSE POINT:** The silanized wafer can be kept at room  
531 temperature indefinitely.
- 532 12. (Optional) Split the wafer into four quarters by scratching with a diamond scribe. Since the wafers  
533 are made of a lattice crystal of silicon, they will break along a well-defined plane.

534 *Sample preparation and imaging protocols for VerCINI (Option A) and  $\mu\text{VerCINI}$  (Option B) are described*  
535 *separately. VerCINI imaging using cells immobilized in agarose cell traps (Option A) is the more common*  
536 *use case, and is straightforward to implement.  $\mu\text{VerCINI}$  (Option B) is more difficult due to more*  
537 *elaborate sample preparation and imaging, and reduced cell loading efficiency, and should only be*  
538 *attempted after users are experienced at standard VerCINI.*

539 **OPTION A: VerCINI sample preparation and imaging**

540 **A.1 Preparation of VerCINI pads. TIMING ~20 – 40 min**

- 541 13. Apply a Gene Frame to a microscope slide. Leave the plastic cover adhered to the Gene Frame  
542 that has a square hole in the middle.
- 543 14. Prepare 10 mL of 6% (w/v) agarose in growth media (with any inducers required) and microwave  
544 until dissolved. Short bursts in the microwave with swirling in between allow bubbles to settle.
- 545 15. After agarose is fully dissolved, place the molten agarose in a 90°C water bath for 5-10 min. Since  
546 the 6% molten agarose is very viscous, this will allow time for bubbles to migrate to the surface  
547 while not allowing the agarose to solidify.
- 548 16. Using wide-bore pipette tips (or cutting the ends off regular ones), apply 800  $\mu\text{L}$  agarose to the  
549 centre of the pillars (Figure 6ai).
- 550 17. Gently but firmly press the microscope slide on top of the agarose (Gene Frame down), aligning  
551 the micropillars with the centre of the Gene Frame (Figure 6aii). Keep the wafer with attached  
552 slide at the temperature at which cells will be imaged. **PAUSE POINT:** Agarose pads should be left  
553 in place on the wafer at the imaging temperature until ready to load with cells.  
554 **?TROUBLESHOOTING.**

555 **A.2 Loading cells into VerCINI pads. TIMING ~10 – 20 min**

- 556 **CRITICAL:** Steps 18-26 should be performed at a constant temperature as much as possible to avoid  
557 perturbations to cell physiology.
- 558 18. Centrifuge 0.5-1 mL of cell culture ( $\text{OD}_{600}$  between 0.3 and 0.5) at 17,000 rcf for 1 min.  
559 Concentration and volume of cells added can be adjusted as required.
- 560 19. Remove supernatant and resuspend in 8-15  $\mu\text{L}$  pre-warmed media.
- 561 20. Using a scalpel, remove agarose slide from the micropillar wafer (Figure 6aiii). To do this, slide the  
562 scalpel between the agarose pad and the wafer, then use the scalpel to lever the agarose pad and  
563 slide away from the wafer. Take care not to disturb the holes or to touch the nanofabricated  
564 pillars. **?TROUBLESHOOTING.**

- 565 21. Place a 9 mm silicone gasket on top of the microholes and spot the concentrated cell culture into  
566 the centre (Figure 6aiv). To prevent evaporation, cover the gasket with a plastic slip and tape it  
567 down to the slide. For this we commonly use the plastic coverslips supplied with Gene Frames,  
568 although many other such covers are possible.
- 569 22. Tape the slide to a flat-bottomed centrifuge rotor with appropriate balance, and centrifuge at  
570 3,220 rcf for 4 minutes (Figure 6aiv). **?TROUBLESHOOTING.**
- 571 23. Wash off excess cells from the top of the pad by holding the pad near-vertically over a waste  
572 container (Figure 6av) and slowly (1 mL/5 s) pipetting fresh, pre-warmed media onto the top of  
573 the agarose pad, allowing the media to flow over the imprinted area and drop into the waste  
574 container. Repeat this step at least 5 times until the majority of excess cells are removed (it is  
575 impossible to remove all of the cells so some excess will still be visible by eye). This step is the  
576 most inconsistent, so can be adjusted through trial and error. **CRITICAL STEP:** If the washing step  
577 is not thorough enough, the pad will be covered in horizontal cells covering up the vertically  
578 immobilized cells (Figure 6b). If the pad is washed too aggressively, the vertically immobilized cells  
579 will be flushed out of the microholes. The washing step is also important to maintain hydration of  
580 the pad after centrifugation.
- 581 24. Allow the pad to air dry until no excess liquid remains (~2 min).
- 582 25. Remove agarose outside the imprinted region by cutting around the imprinted region using a  
583 scalpel. This ensures sufficient oxygen supply to the cells once the coverslip is applied (Figure 6avi).
- 584 26. Peel off the remaining plastic from the Gene Frame and apply the coverslip. Ensure the coverslip  
585 is fully adhered to the Gene Frame by pressing down around all the edges.

### 586 **A.3 Imaging with VerCINI. TIMING 10 min – 12 hr**

587 **CRITICAL:** If doing live-cell imaging, Steps 27-33 should be done with a microscope that is surrounded  
588 by an incubation box pre-heated to the cell growth temperature. Failure to do so can result in  
589 temperature shock to the cells, compromising results.

- 590 27. Transport the slide to the microscope in a pre-warmed empty pipette tip box to reduce  
591 temperature fluctuations in the sample.
- 592 28. Mount the slide on the microscope, preferably with a low autofluorescence immersion oil such as  
593 Olympus Type-F.
- 594 29. Using brightfield illumination, identify an area of the VerCINI slide with a high loading efficiency  
595 and a low number of horizontal cells on top of the pad. **?TROUBLESHOOTING.**
- 596 30. Using fluorescence microscopy, take snapshots to scan the Z-plane to find the structure you wish  
597 to image. Keep the number of snapshots to a minimum to avoid photobleaching. It is often useful  
598 to take a Z-stack image of the entire cell to ensure the correct structure and plane are imaged.
- 599 31. Set focus lock to the optimal Z-plane.
- 600 32. Record a short brightfield time lapse as a control. This allows later identification of wobbling cells  
601 which can affect apparent protein dynamics. We recommend recording ~20 frames over ~1 s.
- 602 33. Record fluorescence with desired settings.

### 603 **OPTION B: $\mu$ VerCINI sample preparation and imaging (ADVANCED)**

#### 604 **B.1 Preparation of $\mu$ VerCINI device. TIMING ~2 hr**

- 605 34. Make a 10:1 ratio of PDMS elastomer base : curing agent by mixing 10 g elastomer base and 1 g  
606 curing agent in a glass or plastic vessel, and stir vigorously.
- 607 35. Degas the mixture by placing it in a vacuum chamber and pulling vacuum for ~15 min.
- 608 36. Pour ~1 mL on top of the silicon micropillars (Figure 7ai).
- 609 37. Place a microscope coverslip on top and press down gently but firmly with a marker cap similar  
610 device with a flat face (Figure 7a<sub>ii</sub>). It is important to press down with enough force to produce a  
611 thin layer of PDMS between the pillars and the coverslip, but not so hard that the pillars may be

- 612 damaged. Cover the back of the coverslip with some remaining PDMS. This will make it easier to  
613 remove some PDMS after baking.
- 614 38. Set the silicon wafer with PDMS and coverslip in an oven and bake at 80°C for 1-2 hrs.
- 615 39. Take the wafer out of the oven and peel off the outer layer of PDMS covering and surrounding the  
616 coverslip. Use a flat-edged blade, such as the bare blade of a utility knife, to slide under and pull  
617 off the PDMS-covered coverslip (Figure 7aiii). Be very careful not to damage the pillars with the  
618 blade while doing this. **PAUSE POINT:** After fabrication,  $\mu$ VerCINI coverslips can be stored at room  
619 temperature indefinitely. **?TROUBLESHOOTING.**
- 620 40. Drill two holes in a glass microscope slide ~15 mm apart diagonally using a power drill equipped  
621 with diamond drill bits. Use a small volume of water to prevent glass dust kicking up during drilling.
- 622 41. Clean the slide to remove glass dust and other impurities by sonicating in ethanol for 15 min and  
623 wiping with a tissue.
- 624 42. Using either a laser engraver or a blade, cut a groove in a piece of double-sided tape to form the  
625 flow channel. The channel must be long enough to reach the inlet and outlet holes, and wide  
626 enough in the centre to accommodate the microhole array.
- 627 43. Adhere the piece of tape to the microscope slide so that the holes line up with the ends of the  
628 channel (Figure 7b). Ensure that the tape seals well by pressing around all the edges. Do not  
629 remove the plastic covering from the other side of the tape.
- 630 44. Take two 10  $\mu$ L pipette tips and cut them in half, keeping the thinnest end. Cut a further ~2-3 mm  
631 from the ends of the tips (where they are thinnest). We find this prevents the tips from protruding  
632 too far through the drilled holes and interfering with fluid flow.
- 633 45. Cut two polyethylene tubes for inlet and outlet tubing. We use 24 cm for the inlet and 67 cm for  
634 the outlet.
- 635 46. Insert the inlet and outlet tubing into the cut pipette tips (Figure 7b) and epoxy them in place.
- 636 47. Insert the cut pipette tips into the drilled holes of the microscope slide on the opposite side from  
637 the double-sided tape (Figure 7b). Ensure that they do not protrude through the holes. Seal the  
638 interface by spreading epoxy between the tip and slide.
- 639 48. Slide a needle into the outlet tubing entrance. **PAUSE POINT:** The microfluidic chamber top can  
640 be stored at room temperature indefinitely. **?TROUBLESHOOTING.**

## 641 **B.2 Loading cells into $\mu$ VerCINI coverslip. TIMING ~10 – 20 min**

642 **CRITICAL:** Steps 49-57 should be performed at a constant temperature as much as possible to avoid  
643 perturbations to cell physiology.

- 644 49. Treat the PDMS-coated coverslip with air or oxygen plasma for 3 min (Figure 7ci). This treatment  
645 renders the PDMS hydrophilic for a relatively short time (a few hours), as material deeper in the  
646 PDMS will eventually migrate to the surface and render it hydrophobic again.
- 647 50. Centrifuge 0.5-1 mL of cell culture ( $OD_{600}$  between 0.3 and 0.5) at 17,000 rcf for 1 min.  
648 Concentration and volume of cells added can be adjusted as required.
- 649 51. Remove supernatant and resuspend in 8-15  $\mu$ L pre-warmed media.
- 650 52. Place a 9 mm diameter silicone gasket on top of the PDMS microholes and spot the cell culture  
651 onto the holes (Figure 7cii).
- 652 53. Place the coverslip on a flat-bottomed centrifuge rotor and cover it with a hard plastic bottle cap  
653 taped down to the plate adapter. This is to prevent significant amounts of liquid evaporation  
654 during centrifugation. Use an appropriate weight balance.
- 655 54. Centrifuge the cells into the holes for 4 min at 3,220 rcf (Figure 7ciii).
- 656 55. Remove the silicone gasket. Rinse off excess cells from the PDMS surface using media by holding  
657 the coverslip upside down over a waste container and gently pipetting 1-2 mL media over the  
658 surface (Figure 7civ). The liquid on the PDMS surface should appear clear. If it remains turbid, rinse



659 with more media. **CRITICAL STEP:** If the washing step is not thorough enough, the pad will be  
660 covered in horizontal cells covering up the vertically immobilized cells (Figure 6b). If the pad is  
661 washed too aggressively, the vertically immobilized cells will be flushed out of the microholes. The  
662 washing step is also important to maintain hydration of the pad after centrifugation.  
663 **?TROUBLESHOOTING.**

664 56. Dab with a tissue to dry off the edges of the PDMS. Be careful not to dry off the region near the  
665 holes themselves. **CRITICAL STEP:** Ensure there is only a thin layer of liquid remaining on top of  
666 the holes. Too much liquid can result in a poorly-sealed chamber as liquid spreads under the  
667 double-sided tape, but too little liquid runs the risk of dehydrating the cells.

668 57. Seal the chamber together by peeling off the plastic covering of the double-sided chamber on the  
669 top of the flow chamber (Figure 7d) and pressing the top of the fluidic chamber to the  $\mu$ VerCINI  
670 coverslip, ensuring that the groove in the tape is over the microholes (Figure 7d). Seal the chamber  
671 fully by pressing around the edges of the tape.

### 672 **B.3 Imaging with $\mu$ VerCINI. TIMING 10 min – 12 hr**

673 **CRITICAL:** If doing live-cell imaging, Steps 58-68 should be done with a microscope that is surrounded  
674 by an incubation box pre-heated to the cell growth temperature. Failure to do so can result in  
675 temperature shock to the cells, compromising results.

676 58. Transport the slide to the microscope in a pre-warmed empty pipette tip box to reduce  
677 temperature fluctuations in the sample.

678 59. Make sure the high working-distance objective is inserted, and use the appropriate immersion oil.

679 60. Position the  $\mu$ VerCINI device above the objective. Place reservoirs of media inside the microscope  
680 incubation box, and place the inlet tubing into one of them. Connect the needle of the outlet  
681 tubing to a 20 mL syringe. Attach the syringe to the syringe pump.

682 61. Fill the chamber with media using the syringe pump operating in Withdraw mode for using the  
683 following settings: diameter = 6", flow rate = 10 mL/s. Ensure media has flowed into the chamber  
684 (~10 s). By operating in Withdraw mode, any failure to seal the chamber will result in the syringe  
685 pump pulling air rather than causing messy leaks in the microscope body. **?TROUBLESHOOTING.**

686 62. Change flow rate to something lower (e.g. 1.1 mL/s) for a slower, steady flow.

687 63. Using brightfield illumination, identify an area of the  $\mu$ VerCINI slide with a high loading efficiency  
688 and a low number of horizontal cells on top of the PDMS. **?TROUBLESHOOTING.**

689 64. Using fluorescence microscopy, take snapshots to scan the Z-plane to find the structure you wish  
690 to image.

691 65. Use an autofocus method of choice to maintain focus lock. We use an image-based system using  
692 a separate infrared brightfield pathway with a custom Micro-Manager plugin<sup>12</sup>, although other  
693 methods may be applied.

694 66. Record a short brightfield time lapse as a control. This allows later identification of wobbling cells  
695 which can affect apparent protein dynamics. We recommend recording ~20 frames over ~1 s.

696 67. Record fluorescence with desired settings.

697 68. To change fluids during imaging, move the inlet tubing from one reservoir to another.  
698 **?TROUBLESHOOTING.**

699 *End of optional protocol steps, remaining protocol steps are common for both VerCINI and  $\mu$ VerCINI.*

### 700 **Image processing and analysis (Common to both VerCINI and $\mu$ VerCINI). TIMING 30 min – 2 hr**

701 69. Select cells that are suitable for subsequent analysis by inspecting raw TIF files in Fiji or ImageJ.

702 a. If a bright-field video was saved, exclude poorly trapped cells (these will appear to wobble in  
703 the holes due to diffusion). If the sample has been characterized previously, poorly trapped  
704 cells can be removed using the fluorescence video.

- 705 b. If a fluorescence Z-stack was saved, exclude cells where signal is not at the correct Z-plane.
- 706 70. Produce videos of cropped, denoised rings using the VerciniAnalysisJ Action Bar.
- 707 a. Draw a 60x60 pixel ROI around each usable cell and record the position in the ImageJ ROI
- 708 Manager. Click 'Save ROIs' to create a compressed folder containing positions of identified
- 709 cells in the same directory as the TIF file.
- 710 b. Click 'Batch denoise+register+crop' and select the directory containing the TIF and zip files.
- 711 The output will be a denoised and registered TIF file of the full FoV and a folder called
- 712 'Indiv\_rings' containing each cell cropped to the selected ROI. *Note*: the denoising step may
- 713 take some time (>0.5 hrs) for large datasets.
- 714 71. Subtract the cytoplasmic backgrounds and produce circumferential kymographs using the
- 715 testVerciniAnalysis script in MATLAB.
- 716 a. Copy and paste the file testVerciniAnalysis.m from the directory ring-fitting2/testing into the
- 717 Indiv\_rings folder.
- 718 b. Open testVerciniAnalysis.m in MATLAB and change any options as required, especially the
- 719 *fname* variable defining the files you want to analyse. More information about options can be
- 720 found in the documentation in the GitHub repository. Detailed documentation of all the
- 721 optional arguments to the VerCINI software may be accessed by typing '*doc verciniAnalysis*'
- 722 or '*doc manualVerciniAnalysis*' in MATLAB. As the VerCINI circle-fitting method is performed
- 723 on a per-frame basis, the analysis method works equally well on septa that constrict
- 724 noticeably over the data acquisition period. In this case, analysis of constriction rate can also
- 725 be performed as the cell radius for each frame is returned as a parameter of the analysis.
- 726 c. Run the testVerciniAnalysis script. A new directory Indiv\_rings/analysed is created containing
- 727 the kymograph (with and without background subtraction), and the background subtracted
- 728 VerCINI movie.

729 **Kymograph analysis. TIMING ~5 – 15 min**

- 730 72. Manually trace individual tracks in kymographs using VerciniAnalysisJ Action Bar in Fiji or ImageJ.
- 731 a. Open the '\_KymoRawWrap.tif' images to analyse.
- 732 b. (Optional) Use 'Ridge Filter' in the Action Bar to highlight ridges in the image.
- 733 c. For each image, use the straight line tool to trace over the kymograph lines and add the trace
- 734 to the ROI manager.
- 735 d. Click 'save ROIs' to create a compressed folder containing the traced lines in the same
- 736 directory as the TIF file.
- 737 73. Once all of the kymographs have been traced, click 'Batch kymotrace statistics'.
- 738 a. Define the camera pixel size and the frame interval of the images, then select the folder
- 739 containing the TIF files and compressed ROI files. The results are output in a new ImageJ
- 740 window and can be saved as a .csv file.
- 741

742 **TROUBLESHOOTING**

Step	Problem	Possible reason	Solution
2	The output from BEAMER is a row/ column of squares rather than a full array	The loops in series performing the translations are only keeping the final loop iteration	Change loop options to merge results of all iterations and repeat
4	The wafer is not uniformly covered with resist	Bubbles in the resist streaked across the wafer	Remove the resist layer by washing the wafer with acetone and repeat the spin-coating, careful to remove bubbles

7	There is still resist in unpatterned regions	The wafer was not developed long enough	Develop the wafer for another ~30 s in MF-321, soak in water, and dry
	All resist was dissolved after development	The wafer was not baked after the pattern was written	Repeat the resist coating, writing, and development (Steps 4-7)
17	The agarose pad is too thick or uneven	The agarose pad solidified too quickly as the microscope slide was pressed down on the wafer	Discard slide. Repeat Steps 13-17. Perform Step 17 on top of a hotplate set to 50°C. The higher temperature will give more time for the agarose to solidify while pressing down
20	The agarose pad stuck to the wafer after removing the slide		Carefully peel the pad off the wafer and set it inside the Gene Frame with holes facing up
22	Cell culture is a dried smear on the pad	Cell culture dried out during centrifugation	Discard pad. Repeat Steps 13-22 with fresh pad, using a silicone gasket to hold the culture in place and a plastic cover to prevent evaporation
29	There are too many horizontal cells on the pad	Cells were not washed off sufficiently after loading	Discard slide. Repeat Steps 13-29, using extra media to wash off unloaded cells
	There are too few cells loaded into holes	Cells were washed off too aggressively after loading	Discard slide. Repeat Steps 13-29, being extra gentle with rinsing off unloaded cells
		Cell culture was not concentrated enough	Discard slide. Repeat Steps 13-29, taking care to concentrate cell culture ~100× before spotting on pad
		Hole widths are too small for cells	Search for a region of the pad with a larger hole size
	Most cells are wobbling in the holes	Hole widths are too large for cells	Search for a region of the pad with a smaller hole size
39	PDMS will not peel off the silicon wafer	The desiccator lost vacuum during the silanisation step, no passivation occurred	Try to carefully remove the PDMS and repeat the silanisation (Step 11)
	The coverslip breaks when peeling it off of wafer	Elastomer base : curing agent ratio was too high	Try to carefully remove the coverslip and repeat Steps 34-39 with lower ratio
	PDMS comes off silicon wafer easily, but will not come off back of coverslip	Elastomer base : curing agent ratio was too low	Discard the PDMS-covered coverslip and repeat Steps 34-39 with higher ratio
48	The needle punctures the tubing	The needle is being pushed while the tip is catching the inside wall of the tubing	Cut off the punctured segment of tubing. Repeat while bending the tubing away from the needle tip to avoid it catching the inside wall

55	Cell culture is a dried smear on the PDMS	Cell culture dried out during centrifugation	Discard coverslip. Repeat Steps 34-39, then Steps 49-55, careful to use a silicone gasket to hold the culture in place and a plastic lid to prevent evaporation
61	The chamber does not fill with media	The chamber is not sealed properly due to liquid under the tape	Discard the device. Repeat Steps 34-61 with a fresh device and, taking care to dry the PDMS outside the hole pattern in Step 56 prior to sealing with tape
		The cut pipette tips are pressed against the PDMS and obstructing flow	Discard the device. Repeat Steps 34-61, careful to cut a few millimetres from the ends of pipette tips before inserting into drilled holes (Step 44)
63	There are too many horizontal cells on the PDMS	Cells were not washed off sufficiently after loading	Flush media through with a high flow rate for ~10 s to dislodge horizontal cells. Otherwise, discard the device and repeat Steps 34-63
	The holes are filled with air bubbles rather than cells	The PDMS is too hydrophobic	Discard the device. Repeat Steps 34-63, careful to treat the PDMS-coated coverslip with plasma (Step 49) before loading cells
	There are too few cells loaded into holes	Cells were washed off too aggressively after loading	Discard device. Repeat Steps 34-63, being extra gentle with rinsing off unloaded cells
		Cell culture was not concentrated enough	Discard device. Repeat Steps 34-63, taking care to concentrate cell culture ~100× before spotting on PDMS
		Hole widths are too small for cells	Search for a region of the PDMS with a larger hole size
	Most cells are wobbling in the holes	Hole widths are too large for cells	Search for a region of the PDMS with a smaller hole size
68	Air is being pulled over tops of cells rather than liquid media	The reservoir of media is empty	Stop imaging. Discard device. Repeat Steps 34-68 using larger reservoir of media and/or lower flow rate
		The inlet tubing is not in the media reservoir	Stop imaging. Discard device. Repeat Steps 34-68, careful that inlet tubing is resting at bottom of reservoir during imaging

743

744 **TIMING**

745 Steps 1-3, design of an array-of-squares pattern: 30 min – 2 hr, depending on speed of user

746 Steps 4-10, fabrication of a silicon micropillar wafer: ~3 hr

747 Steps 11-12, passivation and dicing of the silicon micropillar wafer: ~12 hr  
748 *Silicon wafer fabrication total (Steps 1-12): ~16 hr*  
749 Steps 13-17, preparation of VerCINI pads: ~20 – 40 min  
750 Steps 18-26, loading cells into VerCINI pads: ~10 – 20 min  
751 Steps 27-33, imaging with VerCINI: 10 min – 12 hr  
752 *VerCINI total (Steps 13-33): 40 min – 12 hr*  
753 Steps 34-48, preparation of  $\mu$ VerCINI device: ~2 hr  
754 Steps 49-57, loading cells into  $\mu$ VerCINI coverslip: ~10 – 20 min  
755 Steps 58-68, imaging with  $\mu$ VerCINI: 10 min – 12 hr  
756  *$\mu$ VerCINI total (Steps 34-68): ~2 – 12 hr*  
757 Steps 69-71, image processing and analysis: 30 min – 2 hr, depending on size of dataset  
758 Steps 72-73, kymograph analysis: ~5 – 15 min  
759 *Analysis total (Steps 69-73): ~30 min – 2 hr*

760

## 761 **ANTICIPATED RESULTS**

762 We have provided a detailed protocol for imaging vertically-confined bacterial cells using both VerCINI  
763 and  $\mu$ VerCINI. Using these methods, structures and biomolecular dynamics along the short axes of  
764 bacterial cells can be observed with high resolution without any special requirements for fluorophores  
765 or imaging modalities. VerCINI methods can also be combined with a wide range of other imaging  
766 methods (e.g. SIM or STORM) to provide greater resolution than is possible with each method  
767 individually.

768 Examples of results that a researcher can expect to obtain from VerCINI can be seen in Figures 1 and  
769 2. With VerCINI, the treadmilling dynamics of the bacterial division protein FtsZ can be imaged with  
770 higher sensitivity than any other approach to-date<sup>12</sup> (Figure 1). Beyond this, VerCINI has also been used  
771 to track single molecules of both elongasome and divisome proteins moving circumferentially around  
772 the cell for minutes (ref <sup>16</sup> and our unpublished results), and to image the constricting division septum  
773 using STORM (ref <sup>17</sup> and our unpublished results). VerCINI also makes it possible to image cell pole  
774 proteins like TlpA at high resolution and SNR (Figure 2), paving the way for super-resolution studies to  
775 reveal the spatial organisation of these regions with unprecedented detail.

776 If researchers choose to use  $\mu$ VerCINI to image cells during antibiotic perturbations, they can expect  
777 to obtain results similar to those shown in Figure 3. We have used  $\mu$ VerCINI to observe the rapid effect  
778 of the FtsZ-targeting antibiotic PC190723 on FtsZ treadmilling dynamics across all stages of cell division.  
779 However,  $\mu$ VerCINI is compatible with many other experimental designs that include imaging during  
780 continual fluid flow or fluid exchange. This can include chemostatic growth<sup>33</sup>, live-to-fixed cell  
781 imaging<sup>34</sup>, or DNA-PAINT<sup>35</sup>.

782

## 783 **CONCLUSION**

784 Light microscopy of bacteria provides a wealth of information about their organisation, but  
785 conventional imaging approaches are limited to viewing bacteria along their long axes only. VerCINI  
786 provides a complementary approach by orienting bacteria vertically and imaging along their short axes,  
787 substantially improving the imaging of many biologically important structures and dynamic processes  
788 in non-spherical bacteria that were previously difficult to observe. VerCINI has already found multiple  
789 applications in high resolution imaging of bacterial spatial organisation in hands of a small number of  
790 early-adopter labs<sup>5,12,13,15-17</sup>. We hope that the methods and protocols presented here will allow many  
791 other labs to use VerCINI to look at diverse questions in bacterial cell biology from a different angle.

792

### 793 **Authorship Contribution Statement**

794 KDW, SM, and CJ performed the experiments. KDW, SM, SH, and CD wrote the paper.

795

### 796 **Acknowledgements**

797 We would like to acknowledge Sergii Pud (TU Delft; now at Twente) for help with wafer design and  
798 nanofabrication, Siddharth Deshpande (TU Delft; now at Wageningen) for help with nanofabrication  
799 and soft lithography, Marc Zuiddam (TU Delft) for help with wafer etching, Henrik Strahl (Newcastle)  
800 for strains and helpful discussions, and Joachim Fritzsche (ConScience AB, Sweden) for helpful  
801 discussions. SH, KDW, CJ, SM acknowledge funding support by a Wellcome Trust & Royal Society Sir  
802 Henry Dale Fellowship [206670/Z/17/Z]. CD acknowledges funding support by from the ERC Advanced  
803 Grants 883684 and 669598, and the NanoFront and BaSyC programs. SM supported by a UK  
804 Biotechnology and Biological Sciences Research Council doctoral studentship.

805

### 806 **Competing Interests**

807 The authors declare no competing interests.

808

### 809 **Data availability**

810 Source data for all figures presented in the paper are available at figshare:

811 <https://doi.org/10.25405/data.ncl.c.5652010.v1>

812

### 813 **Code availability**

814 Custom software is available on the Holden lab GitHub page or Zenodo:

815 [https://github.com/HoldenLab/VerCINI\\_nanofab](https://github.com/HoldenLab/VerCINI_nanofab)<sup>36</sup>

816 <https://github.com/HoldenLab/DeepAutoFocus><sup>37</sup>

817 <https://github.com/HoldenLab/VerciniAnalysis><sup>38</sup>

818 <https://github.com/HoldenLab/ring-fitting2><sup>29</sup>

819

### 820 **References**

- 821 1. Huang, B., Babcock, H. & Zhuang, X. Breaking the Diffraction Barrier: Super-Resolution Imaging of  
822 Cells. *Cell* **143**, 1047–1058 (2010).
- 823 2. Pasquina-Lemonche, L. *et al.* The architecture of the Gram-positive bacterial cell wall. *Nature*  
824 **582**, 294–297 (2020).
- 825 3. Garner, E. C. *et al.* Coupled, Circumferential Motions of the Cell Wall Synthesis Machinery and  
826 MreB Filaments in *B. subtilis*. *Science* **333**, 222–225 (2011).
- 827 4. Domínguez-Escobar, J. *et al.* Processive Movement of MreB-Associated Cell Wall Biosynthetic  
828 Complexes in Bacteria. *Science* **333**, 225–228 (2011).
- 829 5. Bisson-Filho, A. W. *et al.* Treadmilling by FtsZ filaments drives peptidoglycan synthesis and  
830 bacterial cell division. *Science* **355**, 739–743 (2017).
- 831 6. Yang, X. *et al.* GTPase activity–coupled treadmilling of the bacterial tubulin FtsZ organizes septal  
832 cell wall synthesis. *Science* **355**, 744–747 (2017).
- 833 7. Kirkpatrick, C. L. & Viollier, P. H. Poles Apart: Prokaryotic Polar Organelles and Their Spatial  
834 Regulation. *Cold Spring Harb. Perspect. Biol.* **3**, a006809–a006809 (2011).
- 835 8. Kuwada, N. J., Traxler, B. & Wiggins, P. A. Genome-scale quantitative characterization of bacterial  
836 protein localization dynamics throughout the cell cycle. *Mol. Microbiol.* **95**, 64–79 (2015).
- 837 9. Laloux, G. & Jacobs-Wagner, C. How do bacteria localize proteins to the cell pole? *J. Cell Sci.*  
838 *jcs.138628* (2014) doi:10.1242/jcs.138628.
- 839 10. Surovtsev, I. V. & Jacobs-Wagner, C. Subcellular Organization: A Critical Feature of Bacterial Cell  
840 Replication. *Cell* **172**, 1271–1293 (2018).
- 841 11. Bowman, G. R., Lyuksyutova, A. I. & Shapiro, L. Bacterial polarity. *Curr. Opin. Cell Biol.* **23**, 71–77  
842 (2011).
- 843 12. Whitley, K. D. *et al.* FtsZ treadmilling is essential for Z-ring condensation and septal constriction  
844 initiation in *Bacillus subtilis* cell division. *Nat. Commun.* **12**, (2021).
- 845 13. Perez, A. J. *et al.* Movement dynamics of divisome proteins and PBP2x:FtsW in cells of  
846 *Streptococcus pneumoniae*. *Proc. Natl. Acad. Sci.* **116**, 3211–3220 (2019).

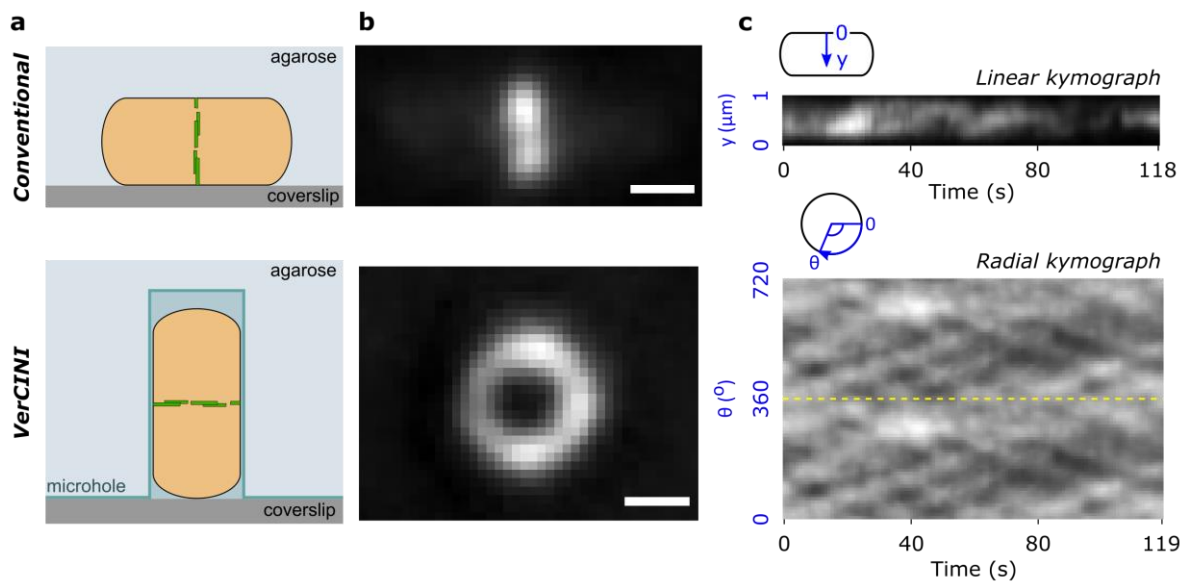
- 847 14. Chai, Y., Norman, T., Kolter, R. & Losick, R. An epigenetic switch governing daughter cell  
848 separation in *Bacillus subtilis*. *Genes Dev.* **24**, 754–765 (2010).
- 849 15. Söderström, B., Chan, H., Shilling, P. J., Skoglund, U. & Daley, D. O. Spatial separation of FtsZ and  
850 FtsN during cell division. *Mol. Microbiol.* **107**, 387–401 (2018).
- 851 16. McCausland, J. W. *et al.* Treadmilling FtsZ polymers drive the directional movement of sPG-  
852 synthesis enzymes via a Brownian ratchet mechanism. *Nat. Commun.* **12**, 609 (2021).
- 853 17. Trouve, J. *et al.* Nanoscale dynamics of peptidoglycan assembly during the cell cycle of  
854 *Streptococcus pneumoniae*. *Curr. Biol.* S0960982221005765 (2021)  
855 doi:10.1016/j.cub.2021.04.041.
- 856 18. Bakshi, S., Choi, H. & Weisshaar, J. C. The spatial biology of transcription and translation in  
857 rapidly growing *Escherichia coli*. *Front. Microbiol.* **6**, 636 (2015).
- 858 19. Zhou, Z. *et al.* The contractile ring coordinates curvature-dependent septum assembly during  
859 fission yeast cytokinesis. *Mol. Biol. Cell* **26**, 78–90 (2015).
- 860 20. Thiyagarajan, S., Munteanu, E. L., Arasada, R., Pollard, T. D. & O’Shaughnessy, B. The fission yeast  
861 cytokinetic contractile ring regulates septum shape and closure. *J. Cell Sci.* jcs.166926 (2015)  
862 doi:10.1242/jcs.166926.
- 863 21. Wollrab, V., Thiagarajan, R., Wald, A., Kruse, K. & Riveline, D. Still and rotating myosin clusters  
864 determine cytokinetic ring constriction. *Nat. Commun.* **7**, 11860 (2016).
- 865 22. Strahl, H. *et al.* Transmembrane protein sorting driven by membrane curvature. *Nat. Commun.* **6**,  
866 (2015).
- 867 23. Briegel, A. *et al.* New Insights into Bacterial Chemoreceptor Array Structure and Assembly from  
868 Electron Cryotomography. *Biochemistry* **53**, 1575–1585 (2014).
- 869 24. Deshpande, S. & Dekker, C. On-chip microfluidic production of cell-sized liposomes. *Nat. Protoc.*  
870 **13**, 856–874 (2018).



- 871 25. de Jong, I. G., Beilharz, K., Kuipers, O. P. & Veening, J.-W. Live Cell Imaging of *Bacillus subtilis* and  
872 *Streptococcus pneumoniae* using Automated Time-lapse Microscopy. *J. Vis. Exp.* 3145 (2011)  
873 doi:10.3791/3145.
- 874 26. Ellefsen, K. L., Dynes, J. L. & Parker, I. Spinning-Spot Shadowless TIRF Microscopy. *PLOS ONE* **10**,  
875 e0136055 (2015).
- 876 27. McGorty, R., Kamiyama, D. & Huang, B. Active microscope stabilization in three dimensions using  
877 image correlation. *Opt. Nanoscopy* **2**, 3 (2013).
- 878 28. Schindelin, J. *et al.* Fiji: An open-source platform for biological-image analysis. *Nat. Methods* **9**,  
879 676–682 (2012).
- 880 29. Seamusholden & Kdwhitl. *HoldenLab/ring-fitting2: v1.1.2.1.* (Zenodo, 2021).  
881 doi:10.5281/ZENODO.4570259.
- 882 30. Luisier, F., Vonesch, C., Blu, T. & Unser, M. Fast interscale wavelet denoising of Poisson-  
883 corrupted images. *Signal Process.* **90**, 415–427 (2010).
- 884 31. Thevenaz, P., Ruttimann, U. E. & Unser, M. A pyramid approach to subpixel registration based on  
885 intensity. *IEEE Trans. Image Process.* **7**, 27–41 (1998).
- 886 32. Jakobs, M. A., Dimitracopoulos, A. & Franze, K. KymoButler, a deep learning software for  
887 automated kymograph analysis. *eLife* **8**, e42288 (2019).
- 888 33. Wang, P. *et al.* Robust Growth of *Escherichia coli*. *Curr. Biol.* **20**, 1099–1103 (2010).
- 889 34. Tam, J. *et al.* A Microfluidic Platform for Correlative Live-Cell and Super-Resolution Microscopy.  
890 *PLoS ONE* **9**, e115512 (2014).
- 891 35. Almada, P. *et al.* Automating multimodal microscopy with NanoJ-Fluidics. *Nat. Commun.* **10**,  
892 1223 (2019).
- 893 36. Whitley, Kevin. *VerCINI\_nanofab.* (Zenodo, 2021). doi:10.5281/ZENODO.5548030.
- 894 37. Whitley, K. D. *et al.* *DeepAutoFocus.* (Zenodo, 2021). doi:10.5281/ZENODO.4573121.
- 895 38. Seamusholden. *HoldenLab/VerciniAnalysisJ: v1.1.1.* (Zenodo, 2021).  
896 doi:10.5281/ZENODO.4617277.

- 897 39. Bisson-Filho, A. W. *et al.* Erratum for the Report: “Treadmilling by FtsZ filaments drives  
898 peptidoglycan synthesis and bacterial cell division”. *Science* **367**, (2020).
- 899 40. Tinevez, J.-Y. *et al.* TrackMate: An open and extensible platform for single-particle tracking.  
900 *Methods* **115**, 80–90 (2017).
- 901

902 **Figures:**

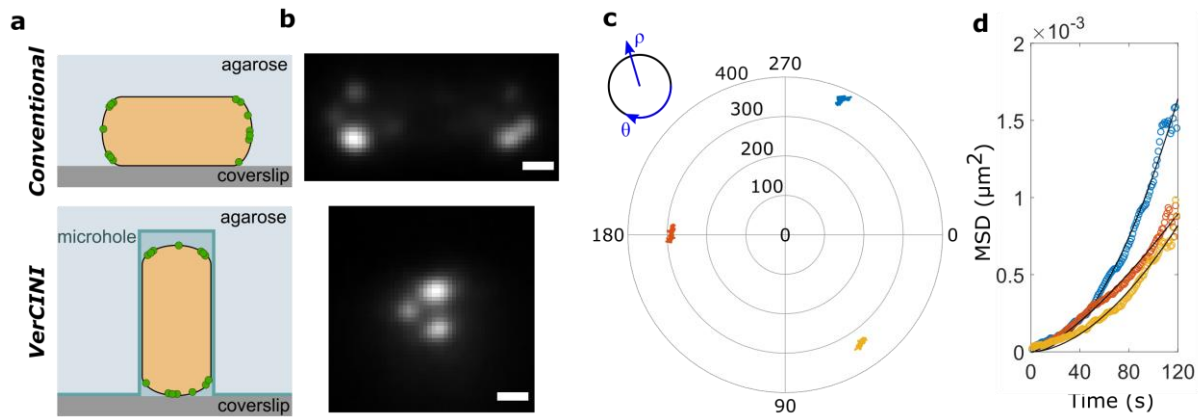


903

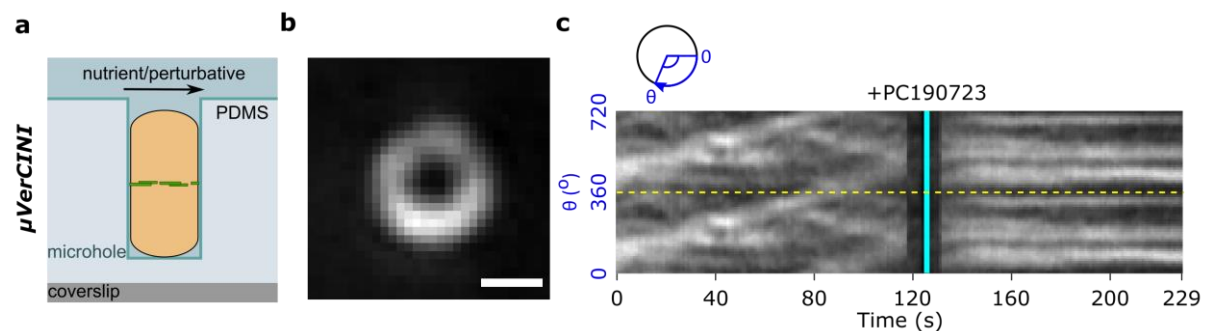
904 **Figure 1: Concept of VerCINI and comparison to conventional imaging of division protein dynamics.**

905 (a) Schematics comparing conventional imaging and VerCINI to image division protein dynamics in rod-  
906 shaped cells. Division rings depicted as green dashed lines. *Top*: A cell lying horizontally under an  
907 agarose pad, with its division ring orthogonal to the microscope coverslip. *Bottom*: A cell confined  
908 vertically in an agarose microhole, with its division ring parallel to the microscope coverslip. (b)  
909 Representative images of *B. subtilis* cells expressing labelled FtsZ. *Top*: TIRF illumination of a cell  
910 expressing mNeonGreen-FtsZ ectopically from an inducible promoter (strain bWM4<sup>39</sup>). The bottom of  
911 the division ring appears as a line across mid-cell. *Bottom*: HiLO illumination of a cell expressing FtsZ-  
912 GFP as a sole copy of FtsZ from the native locus (strain SH130<sup>12</sup>). The full division ring appears as a  
913 circle. Scale bars: 500 nm. (c) Kymographs of FtsZ treadmilling dynamics from cells in (b). *Top*:  
914 Kymograph of mNeonGreen-FtsZ treadmilling dynamics from 0-1  $\mu\text{m}$  across the short axis of the cell.  
915 Diagonal lines show directional motion across the short axis of the cell. *Bottom*: A kymograph of FtsZ-  
916 GFP treadmilling dynamics around the cell circumference. Two full revolutions around the cell (0-720 $^\circ$ )  
917 are plotted side-by-side to resolve filament trajectories that cross 0 $^\circ$ /360 $^\circ$ , separated by a yellow  
918 dotted line. Diagonal lines show directional motion around the full circumference of the cell. Raw data  
919 from Whitley, Jukes et al. (2021)<sup>12</sup>.

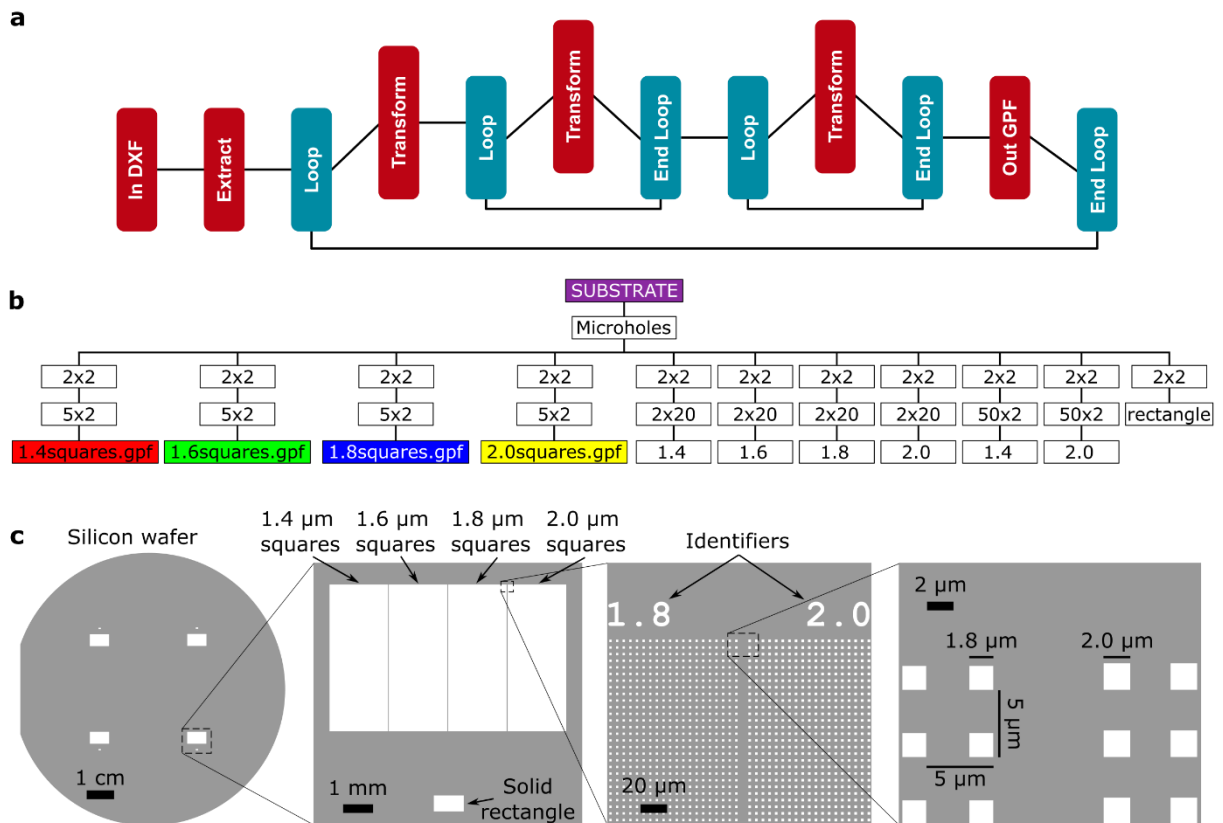
920



921  
 922 **Figure 2: Concept of VerCINI and demonstration to conventional imaging of polar protein dynamics.**  
 923 (a) Schematics comparing conventional imaging and VerCINI to image polar proteins in rod-shaped  
 924 cells. Polar proteins are depicted as green circles. *Top*: A cell lying horizontally under an agarose pad,  
 925 with its poles orthogonal to the microscope coverslip. *Bottom*: A cell confined vertically in an agarose  
 926 microhole, with its poles parallel to the microscope coverslip. (b) Representative images of *B. subtilis*  
 927 cells expressing TlpA-mGFP ectopically from an inducible promoter (strain HS48<sup>22</sup>; Supplementary  
 928 Methods). *Top*: Using conventional imaging with HiLO illumination the proteins appear as unresolved  
 929 blobs at cell poles. *Bottom*: Using VerCINI with TIRF illumination, the proteins appear in several discrete  
 930 clusters. Scale bars: 500 nm. (c) Polar plot showing the motion of TlpA-mGFP clusters from the VerCINI  
 931 imaging in panel (b). Motion of clusters tracked using TrackMate<sup>40</sup>. (d) Mean squared displacements  
 932 of clusters in (c) for different time intervals (circles; colours correspond to those in (c)) with fits to  
 933 generalized diffusion equation  $\langle r^2(t) \rangle = K_\alpha t^\alpha$  (black lines).

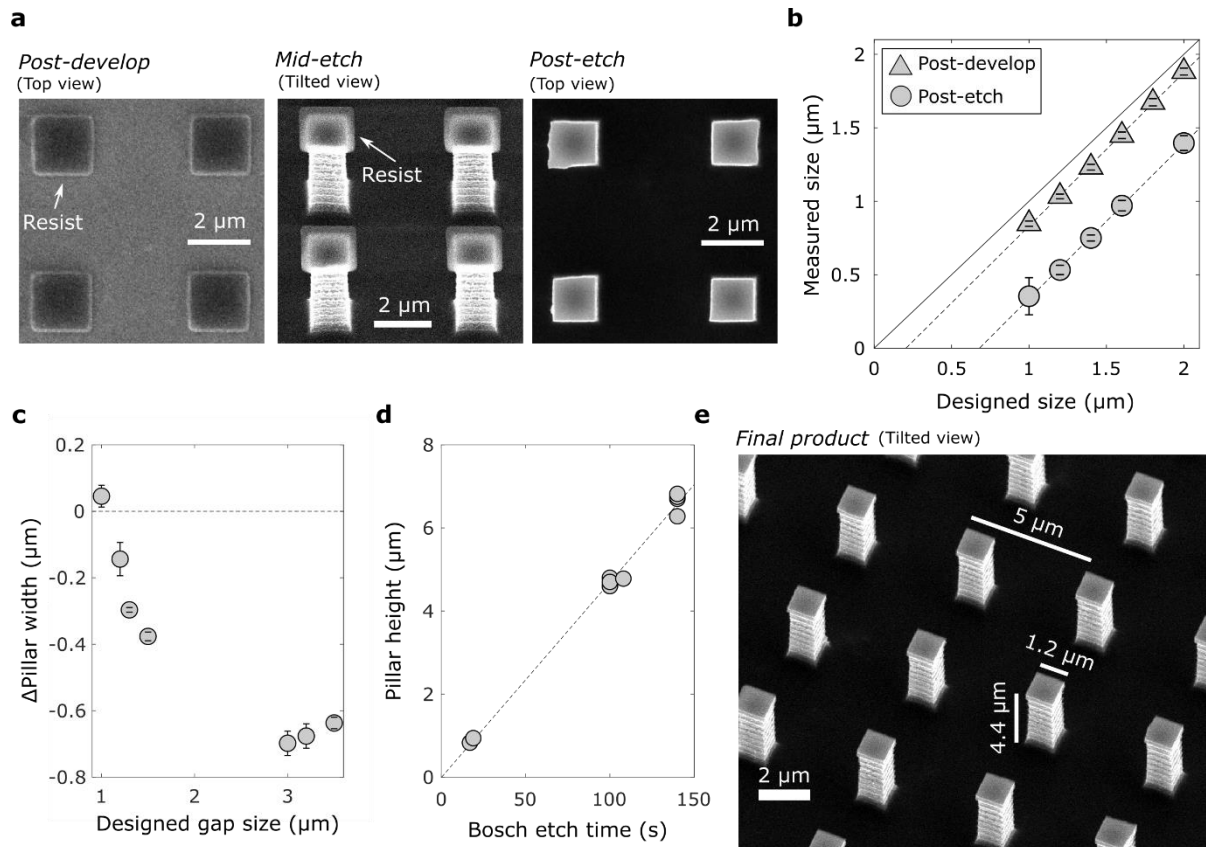


934 **Figure 3: Concept of  $\mu\text{VerCINI}$  and demonstration of imaging division protein dynamics during rapid**  
 935 **antibiotic perturbation.** (a) Schematic depicting a cell confined vertically in an open-topped PDMS  
 936 microhole inside a microfluidic chamber, with its division ring (green dashed lines) parallel to the  
 937 microscope coverslip. (b) Representative image of a *B. subtilis* cell expressing FtsZ-GFP as a sole copy  
 938 of FtsZ from the native locus (strain SH130<sup>12</sup>). The division ring appears as a circle. Scale bar: 500 nm.  
 939 (c) Kymograph of FtsZ-GFP treadmilling dynamics from the cell in (b) around the cell circumference,  
 940 during perturbation with the FtsZ-specific inhibitor PC190723 (cyan line). Two full revolutions around  
 941 the cell (0-720°) are plotted side-by-side to resolve filament trajectories that cross 0°/360°, separated  
 942 by a yellow dotted line. Diagonal lines pre-treatment show directional motion around the full  
 943 circumference of the cell, while horizontal lines post-treatment show static clusters. Raw data from  
 944 Whitley, Jukes et al. (2021)<sup>12</sup>.

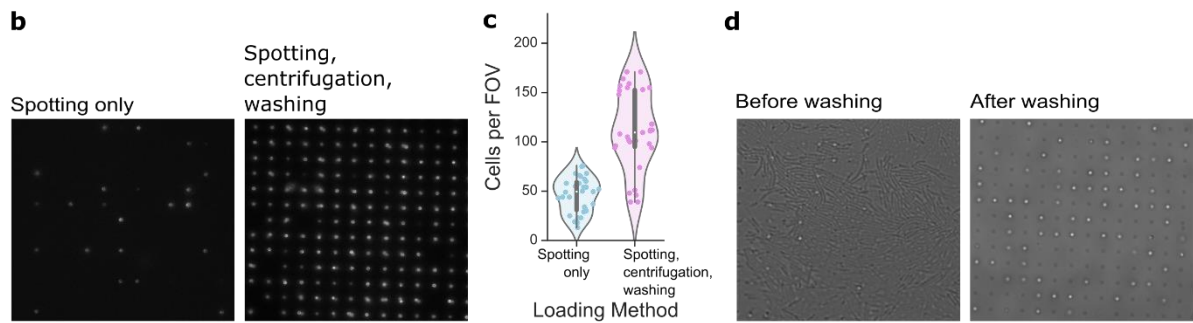
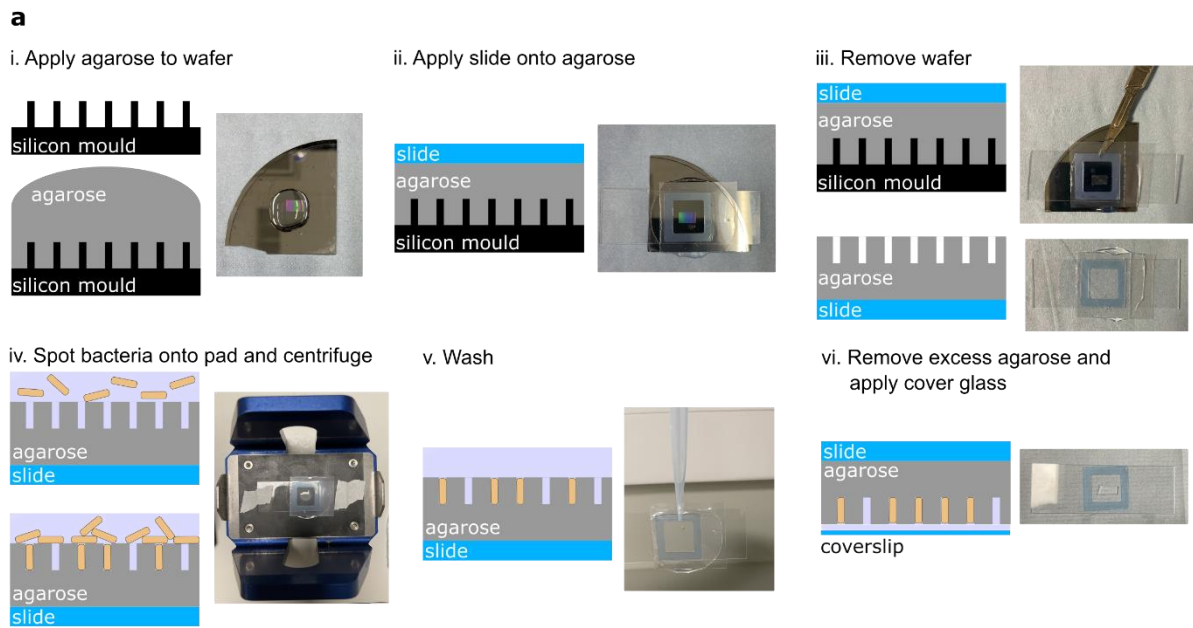


945 **Figure 4: Design of micropillar wafer.** (a) Algorithm of LayoutBEAMER used to produce arrays of  
 946 squares the size of the e-beam machine's main field. (b) Algorithm of Cjob used to produce full arrays  
 947 of squares of four different sizes in each quadrant of a wafer, along with identifiers and solid rectangle  
 948 for measuring height after etching. (c) Output of Cjob code and overall design of silicon wafer showing  
 949 arrays of squares of four different sizes in each quadrant of the wafer, along with identifiers and solid  
 950 rectangle.

951

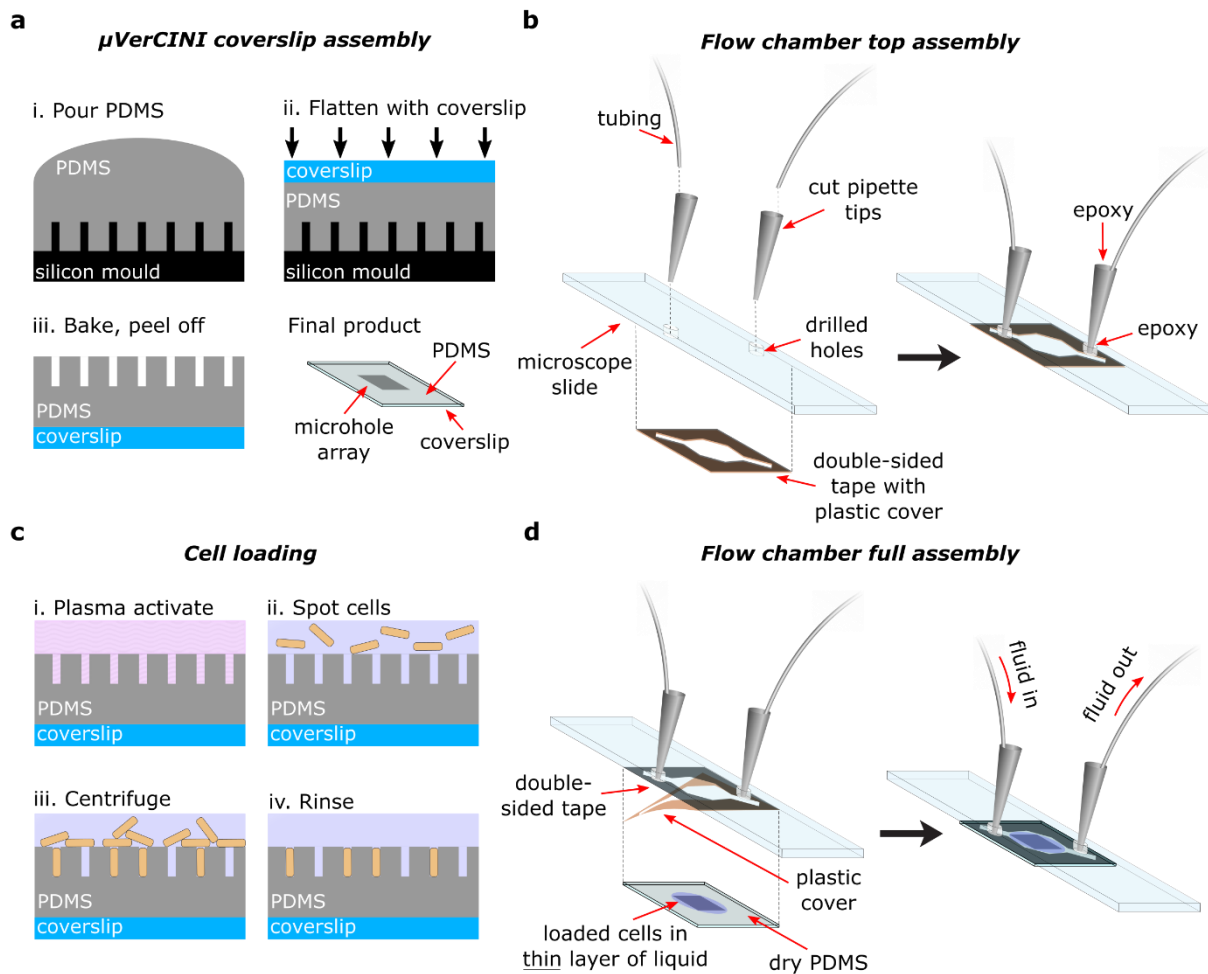


952 **Figure 5: Development and etching of micropillar wafer.** (a) SEM image of silicon wafer with squares  
 953 with designed edge lengths of 2.0  $\mu\text{m}$  during development and etching. *Left panel:* Patterned squares  
 954 of e-beam resist remaining after development, seen from top down. *Middle panel:* Patterned squares  
 955 after several cycles of Bosch etch, but before removing resist with oxygen plasma, seen from a tilted  
 956 angle. Etching produces significant undercutting. *Right panel:* Patterned squares after etching and  
 957 oxygen plasma to remove resist, seen from top down. Scale bars: 2  $\mu\text{m}$ . (b) Comparison of designed  
 958 square sizes to measured square sizes after development (triangles) and after 100 s of Bosch etch  
 959 (circles). Solid line shows hypothetical 1:1 correlation. Dotted lines show linear fits to post-develop and  
 960 post-etch data. Error bars are SD. (c) Change in widths of pillars after 140 s Bosch etch compared to  
 961 designed size of gaps between pillars. Error bars are SD. (d) Effect of etch duration on final heights of  
 962 micropillars. Each circle represents a separate wafer or wafer quarter. Wafers had different square  
 963 sizes, but all had spacing of 5  $\mu\text{m}$ . Dotted line: linear fit to data. (e) SEM image of a final silicon  
 964 micropillar wafer with measured widths  $\sim$ 1.2  $\mu\text{m}$  and spacing 5  $\mu\text{m}$  (and hence gap of 3.8  $\mu\text{m}$  between  
 965 pillars). Heights were measured to be 4.4  $\mu\text{m}$  from profilometer.



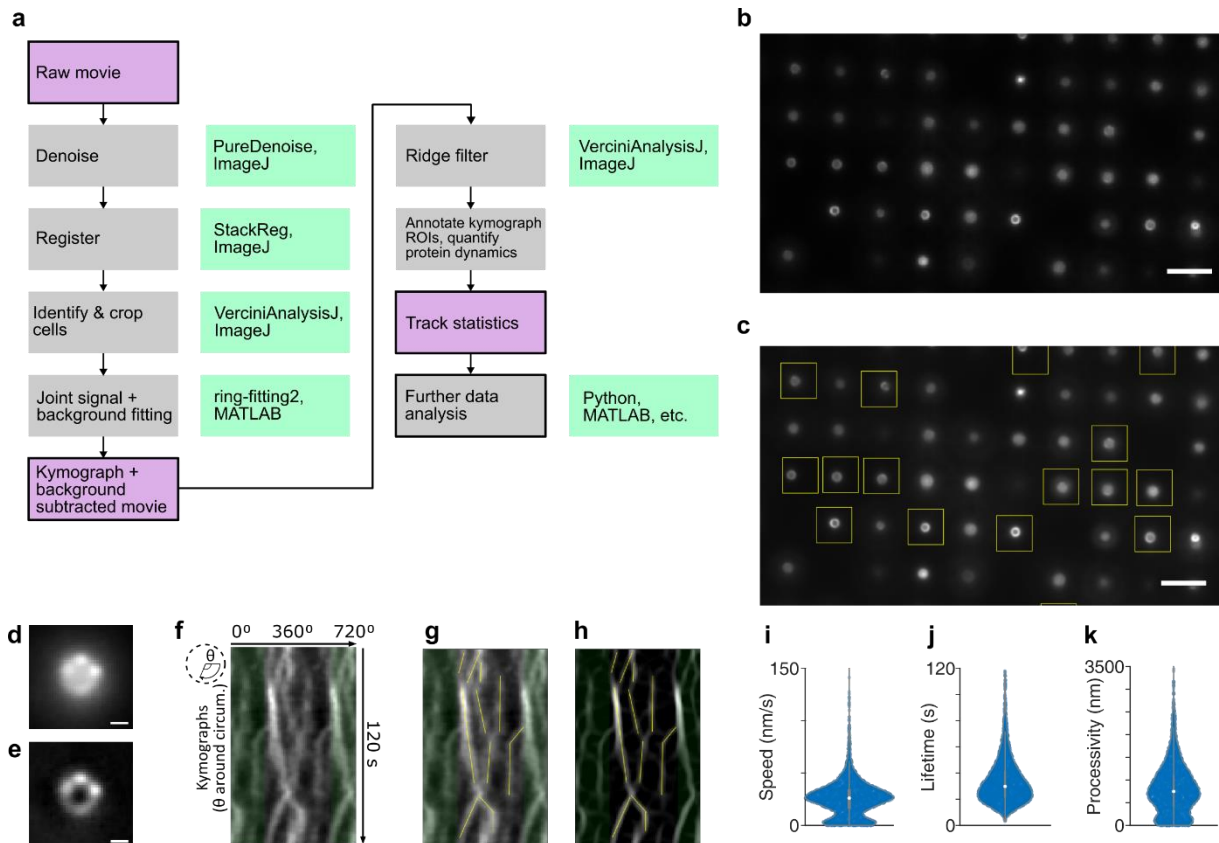
967 **Figure 6: Sample preparation for VerCINI.** (a) Sample preparation workflow. (i) Molten agarose is  
 968 applied to the silicon micropillar wafer. (ii) The cover slide is applied onto the agarose with Gene Frame  
 969 down. (iii) The micropillar wafer is removed from the agarose slide. (iv) Concentrated bacteria are  
 970 pipetted onto the imprinted agarose, and the slide is centrifuged to increase loading efficiency. (v)  
 971 Excess horizontal cells are washed off the pad. (vi) Excess agarose is cut away from the pad, leaving  
 972 only the microhole imprinted area and the cover glass is applied. (b) HILO VerCINI of *B. subtilis* cells  
 973 expressing FtsZ-GFP (strain SH130<sup>12</sup>) loaded into microholes with or without centrifugation. *Left*: cells  
 974 loaded only by spotting liquid culture onto the VerCINI pad and applying the coverslip. *Right*: cells  
 975 loaded by spotting concentrated liquid culture, centrifuging, and washing off unloaded cells. (c) Violin  
 976 plots comparing of loading efficiency between the two loading methods shown in (b). White circles,  
 977 median; thick grey lines, interquartile range; thin grey lines, 1.5x interquartile range. (d) Brightfield  
 978 images of SH130, before and after the washing step.

979



980 **Figure 7: Device assembly and cell loading for  $\mu$ VerCINI.** (a) Assembly of  $\mu$ VerCINI coverslip. (i) Degassed PDMS in a 10:1 elastomer base : curing agent ratio is poured onto silicon micropillars. (ii) A coverslip is pressed firmly down on top of the PDMS to form as thin a layer as possible. (iii) The PDMS is baked in an oven and peeled off to produce a coverslip with open-topped PDMS microholes. The final product can be stored for months to years. (b) Assembly of top of flow chamber. A microscope slide has holes drilled into it. Cut pipette tips are inserted into these holes and epoxied in place, and tubing is inserted into the cut pipette tips and epoxied in place. A piece of double-sided tape with plastic cover still attached has a groove cut into it and is adhered to the microscope slide. The final product can be stored for months to years. (c) Loading cells into open-topped microholes. (i) PDMS is rendered hydrophilic through treatment with air or oxygen plasma. (ii) Cell culture is concentrated and added on top of the microholes. (iii) The  $\mu$ VerCINI coverslip with concentrated cell cultures is centrifuged to load cells into holes. (iv) Cells not loaded into holes are rinsed off with fresh media. (d) Assembly of full flow chamber with loaded cells. PDMS  $\mu$ VerCINI coverslip is dried around the edges, and all but a thin layer of liquid is left above the loaded cells. The plastic cover of the double-sided tape is removed and the tape is adhered to the PDMS. The final product is a closed chamber through which fluid can be flowed.





997 **Figure 8: Image processing and analysis for VerCINI and  $\mu$ VerCINI.** (a) VerCINI image processing  
 998 workflow diagram. Purple box, data. Grey box, Image/ data processing step. Green box, software tool  
 999 to perform image/ data processing step. (b) Exemplar VerCINI image of *B. subtilis* cells expressing FtsZ-  
 1000 GFP. Scale bar, 5  $\mu$ m. (c) Regions of interest around in-focus cell septa/ circumference are manually  
 1001 identified and cropped for further analysis. Scale bar, 5  $\mu$ m. (d) Exemplar denoised VerCINI image of a  
 1002 single cell. Scale bar, 0.5  $\mu$ m. (e) Background subtracted image using joint model-based VerCINI fitting  
 1003 and background subtraction algorithm. (f) Kymograph around septum of background subtracted cell  
 1004 in e. (g-h) Annotated raw kymograph (g) and ridge-filtered kymograph (h). Line ROIs indicate manually  
 1005 detected and annotated filament trajectories. Green regions in f-h indicate repeated section of  
 1006 kymograph added to visualise filament trajectories crossing the boundary of the circular profile. (i-k)  
 1007 Exemplar violin plots of FtsZ-GFP filament dynamics measured by VerCINI. White circles, median; thick  
 1008 grey lines, interquartile range; thin grey lines, 1.5x interquartile range. Raw data in panels b-k from  
 1009 Whitley, Jukes et al. (2021)<sup>12</sup>.

1010

1011 **Supplementary Information** contains methods specific for the data presented in Figure 2, including  
1012 sample preparation, imaging, and data analysis.

1013 **Supplementary Video 1: Suboptimal cell trapping visualized by brightfield microscopy.** *B. subtilis*  
1014 PY79 cells improperly trapped in microhole arrays where microhole width ( $>1.1\ \mu\text{m}$ ) is too large to  
1015 immobilize most cells. Lateral diffusive motion in the holes (wobbling) can be observed in  $\sim 50\%$  of  
1016 trapped cells. The video shows acceptable but not excellent cell loading efficiency. A few cells can be  
1017 seen sitting on top of rather than within microholes, likely those that did not wash off during sample  
1018 preparation. Video was recorded at 100 Hz and plays in real time. Scale bar:  $10\ \mu\text{m}$ .